

**DEVELOPMENT AND EVALUATION OF LOW-COST INFRARED IMAGING
BASED SYSTEM FOR ASSESSING INFLAMMATORY ACTIVITY RELATED
TO RHEUMATOID ARTHRITIS**

THESIS
SUBMITTED IN PARTIAL FULFILLMENT OF
THE REQUIREMENTS FOR
THE DEGREE OF
MASTER OF SCIENCE (ELECTRICAL ENGINEERING)

AT THE

NEW YORK UNIVERSITY
TANDON SCHOOL OF ENGINEERING

BY

SYED SALMAN RAHMAN

JANUARY 2023

DEVELOPMENT AND EVALUATION OF LOW-COST INFRARED IMAGING BASED SYSTEM
FOR ASSESSING INFLAMMATORY ACTIVITY RELATED TO RHEUMATOID ARTHRITIS

THESIS
SUBMITTED IN PARTIAL FULFILLMENT OF
THE REQUIREMENTS FOR
THE DEGREE OF
MASTER OF SCIENCE (ELECTRICAL ENGINEERING)
AT THE
NEW YORK UNIVERSITY
TANDON SCHOOL OF ENGINEERING
BY
SYED SALMAN RAHMAN
JANUARY 2023

APPROVED:



Dr. Matthew Campisi

Jan 4, 2023

Date


Dr. Ivan Selesnick

January 4, 2023

Date

Microfilm or other copies of this thesis are obtainable from

UMI Dissertation Publishing

ProQuest CSA

789 E. Eisenhower Parkway

P.O. Box 1346

Ann Arbor, MI 48106-1346

VITA

Syed Salman Rahman was born on the 3rd of February 1997 in Feni, Bangladesh. He holds a Bachelor's degree in Electrical-Mechatronics from Universiti Teknologi Malaysia, Malaysia (graduated 2020). Following a year of professional experience, he enrolled in Masters of Science (Electrical Engineering) at the NYU Tandon School of Engineering in September 2021. He is currently working as an Application Engineer at STMicroelectronics. This work was completed at the Student Impact Innovation Lab (SIIL) over the course of 10 months, February 2022 and December 2022.

DEDICATION

I dedicate this to all people who suffer from Rheumatoid Arthritis every single day like my father.

ACKNOWLEDGEMENTS

My mother and my sister for being the greatest support line I could ask for. My fellow colleagues at the Impact Innovation Lab for their outmost support, and Prof. Campisi for introducing this topic to me. Lastly, eliya for constantly pushing me to finish this thesis.

Abstract

**DEVELOPMENT AND EVALUATION OF LOW-COST INFRARED IMAGING
BASED SYSTEM FOR ASSESSING INFLAMMATORY ACTIVITY RELATED TO
RHEUMATOID ARTHRITIS**

By

Syed Salman Rahman

Advisor: Dr. Matthew Campisi, PhD

**SUBMITTED IN PARTIAL FULFILLMENT OF THE REQUIREMENTS FOR
THE DEGREE OF MASTER OF SCIENCE (ELECTRICAL ENGINEERING)**

JANUARY, 2023

Rheumatoid Arthritis (RA) is an auto-immune disease in which inflammation plays a vital role. In the United States of America alone, around 1.3 million people are affected by RA [45]. Traditionally, imaging techniques such as X-ray, ultrasound (US), and Magnetic Resonance Imaging (MRI) are used to detect the progression of RA by visualizing structural changes in the joints. These methods come with the disadvantages of being inaccessible, high cost to perform, and not being able to visualize changes in the temperature of the tissues [49]. There is a clinical need for a low-cost, non-invasive imaging tool that can detect inflammation in the joints of people with inflammatory arthritis. Although there have been few attempts to use this technology as potent low-cost sensing devices in non-invasive medical devices, Infrared Thermal Imaging (IRT) has been widely used in heavy and expensive industrial and military engineering. IRT provides a way to measure temperature differences in space and gives an output of a temperature field from which fine-grained feature detection can be obtained which can be evaluated after pharmacological, physical, or surgical treatment [60]. In this study, the IRT-based system was developed using FLIR Lepton 2.5 thermal camera which utilizes an 80x60 Long Wave Infrared (LWIR)

micromechanical sensor array, a fixed-focus lens assembly, and signal-processing electronics all combined in one infrared camera system. The study suggests different methodologies and technologies for acquiring and analyzing images.

CONTENTS

Vita	iii
Dedication	iv
Acknowledgments	v
Abstract	vi
List of Figures	xi
List of Tables	xiii
1 Introduction	1
1.1 Introduction	1
1.2 Scope	2
1.3 Format	3
2 Background	4
2.1 Rheumatoid Arthritis	4
2.1.1 Diagnosis of RA	6
2.2 Infrared Thermography	6
2.2.1 Operating principle of thermal infrared imaging	7

2.2.2	Long-Wave Infrared	8
2.2.3	Micro-Bolometer	8
2.2.4	Related Work	9
2.3	Traditional Methods for Detecting RA	11
2.3.1	MRI	11
2.3.2	Ultrasound	12
2.3.3	X-ray	13
2.3.4	CT Scan	14
2.4	Embedded Systems	14
2.4.1	Micro-controllers	15
2.4.1.1	ARM Cortex M4	15
2.4.2	Wireless Communication	16
2.5	BlackBody Testing	16
3	Methodology	19
3.1	System Architecture	19
3.1.1	System Flowchart	20
3.1.2	FLIR Lepton image characteristics	22
3.2	Image analysis technique	24
3.2.1	Lepton raw data to thermal image	24
3.2.2	Thermal color image to thermal grayscale image	25
3.3	System Components	25
3.3.1	FLIR Lepton 2.5	26
3.3.2	Teensy 3.2	26
3.3.3	ESP12-S	27
3.3.4	Peltier Module	28

3.4	System Design and Implementation	29
3.4.1	Physical Connection	29
3.4.2	Implementation of Serial Communication (FLIR Lepton - Lepton3.2)	32
3.5	Data Acquisition	33
3.5.1	SPI Communication: Teensy and Lepton	33
3.5.2	Serial Communication: Teensy and ESP-12S	35
4	Results and Discussion	37
4.1	Initial Experiments	37
4.2	Discussion	47
5	Conclusion and Future Works	48
5.1	Project Overview	48
5.2	Future Work	48
	Bibliography	50

LIST OF FIGURES

2.1	Physio-pathological changes in a healthy joint vs. rheumatoid arthritis joint	5
2.2	Principle construction of an infrared image using microbolometer [17]	11
2.3	Electromagnetic Spectrum	12
2.4	Basic Architecture of an Embedded System	15
3.1	System Architecure	19
3.2	Data collection phase system flowchart	21
3.3	Full system flowchart	22
3.4	FLiR Lepton 2.5 and Teensy 3.2 Schematic	23
3.5	1 video line per 160-byte payload	23
3.6	Video Packet Contents Per Frame	23
3.7	FLiR Lepton 2.5 and Teensy 3.2 Schematic	24
3.8	Flow of Thermal Image Conversion	25
3.9	Physical connection between Teensy and ESP shield	31
3.10	Physical connection between Teensy and Lepton	31
3.11	SPI communication: Lepton and Host (Teensy) [18]	33
3.12	Illustration of SPI Mode 3[18]	33
3.13	Data acquisition model	34
3.14	Communication between Teensy and ESP shield	36

4.1	Image of noisy background	38
4.2	Image from default colormap	38
4.3	RGB Plot of the Colormap used	39
4.4	Hand Position 1	39
4.5	Histogram of thermal image in position 1	40
4.6	Hand Position 2	41
4.7	Histogram of thermal image in position 2	42
4.8	Hand Position 3	42
4.9	Histogram of thermal image in position 3	43
4.10	Hand Position 4	43
4.11	Histogram of thermal image in position 4	44
4.12	Hand Position 5	44
4.13	Histogram of thermal image in position 5	45
4.14	Hand Position 6	45
4.15	Histogram of thermal image in position 6	46

LIST OF TABLES

2.1	Literature Review of IRT-based RA diagnosis	10
3.1	Key Specifications of Lepton 2.5	26
3.2	Key Specifications of Teensy 3.2 [43]	27
3.3	Key Specifications of ESP-12S [54]	28
3.4	Key Specifications of Peltier Module [57]	29
3.5	Physical pin connection (Lepton-Teensy)	30
3.6	Physical pin connection (ESP-Teensy)	30

1 | INTRODUCTION

1.1 INTRODUCTION

Rheumatoid arthritis (RA) is a chronic, autoimmune condition that predominantly occurs in the synovial tissue. RA is known to affect approximately 5 million patients around the world. Only in the United States of America, approximately of 1.3 million suffer from this deadly disease. RA is diagnosed on the basis of clinical, radiological, and biological findings as defined by the American College of Rheumatology (ACR) [22]. There are several diagnostic tools and methods currently practiced for the diagnosis of RA, like Computed tomography (CR), magnetic resonance imaging (MRI), ultrasound (US), and photoacoustic imaging (PAI) but these imaging modalities come with their specific and objective drawbacks when it comes to detecting joint inflammation. For instance, CR does not have the capability to detect any sort of soft tissue synovitis and bone erosion occurring at an early stage. While techniques like MRI and CR could be beneficial in the extraction of information on soft tissue abnormalities and bone erosion, they are highly dependent on extensive training and competence of the operators which not only leads these techniques to high cost with limited availability but also make the reproducibility of the images to be unsatisfactory. [10], [16]. It is noted that if targeted therapy that utilizes a combination of Disease-modifying antirheumatic drugs (DMARDs) can be provided in the first 3 months of diagnosis, it can dramatically improve long-term patient outcomes [30]. Similar study reports that over 20 to 30 percent of RA patients eventually end up with irreversible disability within

the first few years of diagnosis [41]. This creates the clinical need for a low-cost, accessible, and fast report-generating system that will help physicians in both diagnosis and observing the progression of RA. Thermal cameras are capable of detecting infrared energy which is a subset of electromagnetic radiation which is often perceived as heat. Since the 1950s, infrared thermography has been utilized in clinical settings to observe the temperature profile for biomedical applications such as fever screening of potentially infected patients, breast cancer detection [28], [3], diabetes neuropathy [6], peripheral vascular disorders detection [46], [25] and in psoriasis arthritis. The earliest modern thermography was used to screen breast tumors, although due to the drawback of less sensitivity and low resolution, it is now mainly used as an alternative method to detect breast tumor mass [29]. Numerous researchers have worked to increase the accuracy of tumor identification by raising camera resolutions, using better algorithms, and creating more advanced tools. In recent years, the role of thermography-based solutions for examining hand joints for diagnosis and prediction of disease progression has been studied. Thermographic images of healthy individuals and RA patients without active inflammation displayed significant differences in temperature distribution over the skin surface [19].

1.2 SCOPE

This thesis will cover several areas within Infrared Imaging and aims to:

1. Performance of the Camera is evaluated through a Blackbody with specific temperature and emissivity
2. The IR camera must be simple to incorporate into embedded devices, able to precisely capture the photos
3. In each pixel of each image, non-contact temperature information should also be provided.

4. Using FLIR Lepton v1.4 camera with a breakout board with Teensy 3.2 Micro-controller microcontroller to capture images and stored them in the cloud.
5. The system must be connected to the Internet in order for the embedded devices to be networked and controlled remotely.
6. The study is required to understand thermal images from both RGB and grayscale images to verify if temperature differences can be realized.

1.3 FORMAT

This thesis is organized into five chapters including the introduction. All the chapters are in chronological order. Chapter 1, primarily discusses the problem background and problem statement of the project. The scope defines the functionalities and constraints of the project. Chapter 2 introduces the background of RA and the theory behind Infrared thermography. It also covers the literature review of methods used for diagnosing RA which is categorized into traditional solutions and state of art solutions. This chapter will also explore the important moving parts underlying the Chapter 3 describes each moving part of the system in detail, including a top-down overview of the system architecture, system implementation, and flowchart. Chapter 5 will conclude the report and list key insights from the experimentation. It also provides an outline for prospective future work in the pipeline.

2 | BACKGROUND

2.1 RHEUMATOID ARTHRITIS

Rheumatoid arthritis is a chronic inflammatory and autoimmune disorder characterized by severe joint and bone damage. It causes synovial joint inflammation along with osteocyte and cartilage degradation. The patient's quality of life is significantly impacted by long-term disability, inability to function in social situations and at work, and higher death rates that follow. Rheumatoid arthritis affects the lining of joints, resulting in an excruciating swelling that may eventually lead to bone erosion and joint deformity, unlike osteoarthritis, which affects the wear-and-tear deterioration of your joints [23]. The metacarpophalangeal and proximal interphalangeal joints, as well as the wrists, are almost invariably affected.

Active RA is characterized by arthralgia, joint degradation, redness, synovitis, and swelling, resulting in complicated autoimmune and inflammatory responses. These symptoms are caused by synovial lining cells and inflamed blood vessels. The absence of the rheumatoid factor (RF) is one of the plasma cell antibodies that play a considerable role in contributing to this disease. Both macrophages and lymphocytes produce pro-inflammatory cytokines and chemokines in the synovium, which include TNF-alpha (tumor necrosis factor), osteoclasts, IF-gamma (interferon gamma), and ILs (interleukin). In progressed RA, thin-lined synovium proliferates and releases various cartilage degradation mediators. These inflammatory mediators contribute actively to consistent inflammation along with cartilage and bone degradation, resulting in RA [34]. Ac-

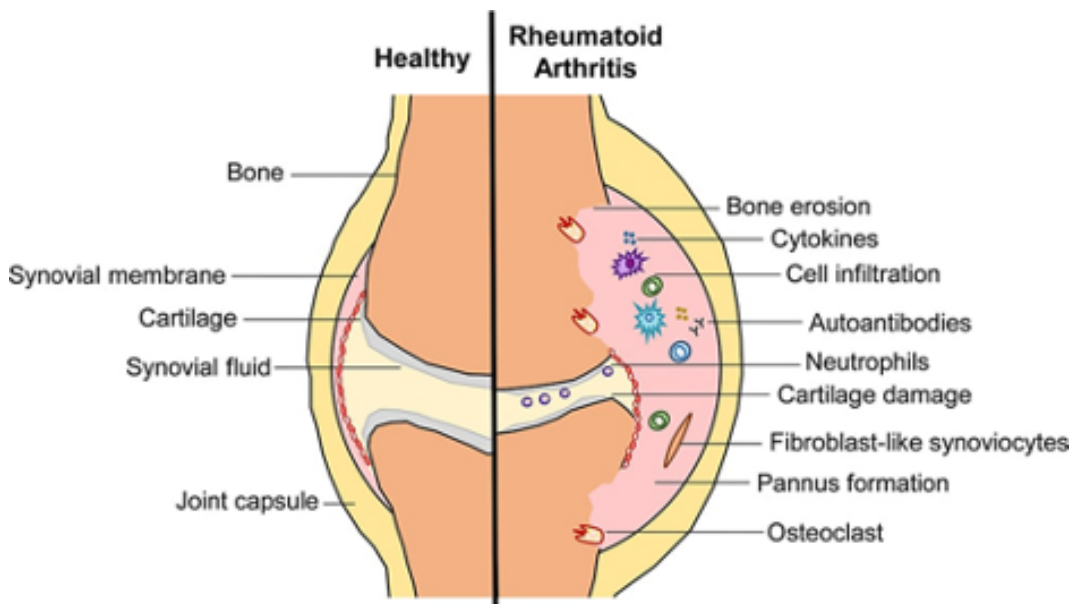


Figure 2.1: Physio-pathological changes in a healthy joint vs. rheumatoid arthritis joint.

cording to the Global Burden of Disease 2010 Study, 0.24 percent of people globally are predicted to have RA. Estimates of the frequency of RA are considerably more significant in the United States and northern European nations, ranging between 0.67 to 1.1 percent. In the United States and northern European countries, the average incidence of RA is around 40 in every 100,000 people. Furthermore, the mortality rate increases for people with RA due to autoimmune injury and chronic inflammation, as other organ systems are also affected simultaneously. The diagnosis of rheumatoid arthritis cannot be confirmed by a single diagnostic test. Several tests can offer factual information that improves diagnostic accuracy and enables the tracking of illness development [44]. There are differences in the type and pattern of affected joints in each patient. The progression of the illness may also change depending on the presence or absence of several factors, such as hereditary background, the frequency of swollen joints, the presence or absence of antibodies in the blood, and the intensity of the inflammatory process [20]. But, due to the absence of treatment within the first two years of disease onset, it may lead to articular damage and bone erosion. Hence, early diagnosis of RA is essential, giving the window of opportunity for accurate treatment initiation, preventing the disease from progressing into some aggressive

form, and requiring any aggressive medications such as immuno-suppressants. Additionally, researchers are working to improve RA biological therapies, which have constantly been developed and effectively applied for the last 30 years. This has had a hugely favorable impact on prognosis and mobility. However, it has changed the emphasis of attention from prevention to treatment or from early diagnosis to therapeutic monitoring. The earlier treatment is optimal in RA, but the treatments still rely on physician-dependent conventional examination techniques, for instance, physical exam, imaging, or synovial biopsy.

2.1.1 DIAGNOSIS OF RA

The diagnosis is not challenging when a patient has typical clinical and radiologic characteristics. The following diagnostic standards have been suggested for unusual cases [47], [2].

1. Stiffness in the morning
2. Symmetrical arthritis pattern
3. Soft tissue swelling
4. Inflammation in the joints especially proximal interphalangeal and metacarpophalangeal
5. Presence of RF by doing a blood test
6. Radiograph showing bone erosion without periarticular osteopenia

Criteria 1–4 must be present for a minimum of 6 weeks. The presence of four or more criteria defines RA.

2.2 INFRARED THERMOGRAPHY

Thermal imaging is a highly robust remote sensing approach for various reasons, primarily when used to clarify field research. As science advances, this technology has come to the fore-

front because of the significant advancements in electronics over several decades. It is used in manufacturing, preventive-predictive management, non-destructive testing, temperature monitoring, etc. It performs well in low light and low visibility situations. In earlier times, thermal imaging was costly as it required a massive cooling system. However, it is now more accessible and usable in many contexts as it doesn't need an enormous cooling system anymore.

2.2.1 OPERATING PRINCIPLE OF THERMAL INFRARED IMAGING

Thermal radiation is a function of the object's temperature. With the help of an array of microbolometers, fundamental means of IR radiation can be measured. Three factors can be measured: Absorption, Transmission, and Emission. The distribution of turning infrared (IR) radiation (heat) into visual pictures that show the spatial distribution of temperature differences in a scene observed by a thermal camera is known as thermal imaging. An infrared detector, often in the form of a focal plane array of micron-sized detecting components or pixels, is installed in the imaging camera. The temperature-dependent emission of electromagnetic radiation occurs in all stuff above absolute zero temperature. The radiation is directly related to an object's internal temperature. Objects begin to release radiated beams of visible light as their temperature rises, starting as a faint red glow until becoming white hot and finally releasing the majority of that energy in ultraviolet and beyond wavelengths. It is believed that radiation is proportional to electrical impulses. The output signal is picked up by the camera and later used to produce images [56].

The adjacent region to visible light spectra and infrared light spectrum is beyond the range of light that the human eye can see. It is in between the visible and microwave light spectral regions. In physics, infrared radiation or light is characterized as one of the electromagnetic waves. IR light is absorbed more directly by matter than other electromagnetic waves, increasing its kinetic energy. Infrared light is usually divided into three categories. They are near-infrared, mid-infrared, and far infrared. Near IR has the wavelength closest to visible light spectra's red

end. The wavelength ranges from 750 nm to 1300 nm. The frequency ranges between 215 THz and 400 THz. The frequency range is 0.3 THz to 20 THz. Near IR produces the least heat. Secondly, mid-IR's wavelength ranged between 1300 nm to 3000 nm and the frequencies ranged between 20THz to 215 THz. Lastly, the wavelength range of the far IR band that is the closest to microwaves and produces the most heat is from 3000 nm to 1mm [24].

2.2.2 LONG-WAVE INFRARED

In Figure 2.3, the three regions generally used for thermography are shown. LWIR regions are referred to as "thermal infrared" for the same reasons mentioned. LWIR collects the light in the 8 μm to 14 μm spectral band and is the wavelength range with the most available thermal imaging cameras. In fact, according to Planck's law, terrestrial targets emit mainly in the LWIR. In the LWIR band there is quite more radiation emitted from terrestrial objects compared to the MWIR band. LWIR systems applications include thermography/temperature control, predictive maintenance, gas leak detection, imaging of scenes, which span a very wide temperature range (and require a broad dynamic range), and imaging through thick smoke.

2.2.3 MICRO-BOLOMETER

A microbolometer is one of the specific types of bolometers that are usually used in thermal cameras. The wavelengths covered by these long infrared detectors range from 8 to 14 nm. This light-sensitive and uncooled thermal sensor absorbs an object's thermal radiation through a thermally insulated membrane. The sensor has three different layers. They are infrared absorbers, a reflective layer, and a silicon substrate. This technology has been constantly used in this field due to its sensitivity to electrical resistance that varies with temperature. The sensing elements inside microbolometers are the thermistors positioned as hanging bridges on top of a readout integrated circuit. The thermally insulated components change the temperature in response to

release heat energy. To minimize the sensitivity error and minor variation in temperature reading, the components are wrapped in premium vacuumed packaging that not only reduces the air gap but also allows the establishment of a conduction channel by dampening sensor sensitivity as stated in [17].

2.2.4 RELATED WORK

Eight (8) studies were found in the literature that studied the application of Infrared Thermography to investigate Rheumatic Diseases in hand joints. [9, 11, 26, 42, 48, 52, 53, 55]

In the studies of [9, 11, 26, 48, 55], a significant difference was reported after statistical analysis was executed using absolute temperature in the joints of two groups of participants of patients affected by rheumatic diseases and healthy controls.

On the contrary, Pauk et al. in [42] observed no significant different in the baseline temperature of fingers in patients with RA compared to their counterparts, healthy individuals. The study however observed a higher contrast between the maximum and minium temperature ($T_{max} - T_{min}$), in other words the temperature scale rises as it goes parallel to the finger's axis. It was also observed that when the post-cooling and post-rewarming were done before the data was collected, temperature $T_{max} - T_{min}$ measured along the finger's line was higher in patients with RA.

Table 2.1 summarizes the the findings from all these 8 studies. One finding was consistent throughtout all the studies, it was of the significant differences in absolute temperature between a healthy and RA patient. In [53], authors proposed a novel method where Ultrasound is sound along with the thermal images as a combination, which showed optimistic result in terms of correlation with DAS-28.

Author-Year-Journal	Findings	Camera
Borojević, N. (2011)[9] Periodicum Biologorum	1. Joints' absolute temperature differences 2. Different patterns of heat intensity distribution	Thermo Tracer TH7102WL
Pauk, J. (2019) [42] Medical & Biological Eng. & Comp.	Higher temp. contrast (Tmax-Tmin) after a cooling test in RA patients	E60bx
Jones, B.(2018)[26] Clinical Rheumatology	1. Joints' absolute temperature differences 2. IRT findings did not associate with clinical measures of disease activity	FLIR T300
Umapathy, S. (2018)[55] Journal of Medical and Biological Eng.	1. Joints' absolute temperature differences 2. the best joints to the image are the MCPs of the second and third fingers	FLIR T400
Capo, A (2015)[11] Microvascular Research Journal	1. Joints' absolute temperature differences 2. IRT findings correlate with pain	FLIR 660sc
Snekhalatha, U. (2015)[48] Journal of Engineering in Medicine	1. Joints' absolute temperature differences 2. The best joints to image are the MCP, the proximal interphalangeal joints, distal interphalangeal joints of the third finger	FLIR T400
Tan YK. (2020)[52] Clinical radiology	Joints in patients have significantly higher temperature readings, verified by US	FLIR T640
Tan YK. (2021)[53] Clinical radiology	Novel use of combined thermal and ultrasound imaging in RA shows superiority to imaging alone in terms of correlation with DAS-28	FLIR T640

Table 2.1: Literature Review of IRT-based RA diagnosis

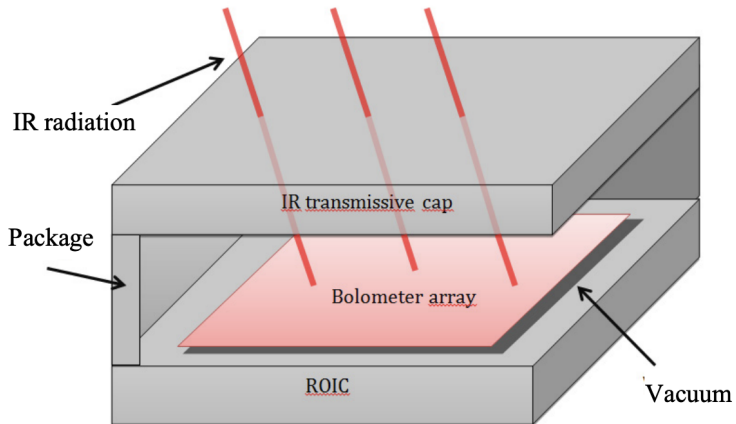


Figure 2.2: Principle construction of an infrared image using microbolometer [17]

2.3 TRADITIONAL METHODS FOR DETECTING RA

2.3.1 MRI

Without ionizing radiation, MRI offers multiplanar tomographic imaging with unprecedented soft tissue contrast, allowing evaluation of all the structures involved in arthritic disease, including the synovial membrane, intra-, and extra-articular fluid collections, cartilage, bone, ligaments, tendons, and tendon sheaths. It has been confirmed to be significantly more effective for identifying the inflammatory disease, especially in its early stages, than clinical examination and X-ray. In a study of metacarpophalangeal (MCP) joints in early and established RA patients, mini arthroscopy confirmed the presence of bone pathology in all joints with MRI bone erosions and histological and macroscopic synovitis in all joints with MRI synovitis. These findings demonstrate the close correlation between MRI and histopathological signs of synovial inflammation [27, 38–40]. When compared to X-rays, MRI has definite advantages, but it also has drawbacks, including higher cost and less access. When the costs of biological RA medication or the indirect costs of sick leave or early retirement are considered, the expenses of MRI make up a substantial amount of the entire cost of treating RA patients. Only one study has found a relationship

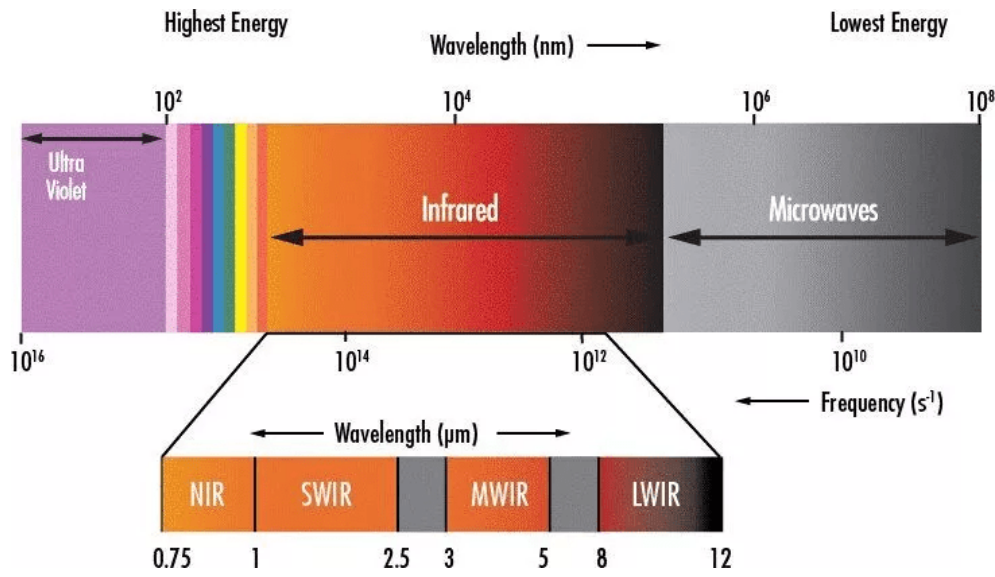


Figure 2.3: Electromagnetic Spectrum

between baseline MRI scans and long-term functional disability. According to findings from the same group, early RA-related substantial MRI bone oedema and wrist erosions anticipated tendon weakening and impaired hand mobility [8, 62]. Another issue with MRI is its ability to forecast the progression of a disease in individuals in clinical remission. Further studies are required to confirm the therapeutic relevance.

2.3.2 ULTRASOUND

Among all other imaging technologies, ultrasound is highly accessible, patient-friendly, and cost-effective. The multiplanar test doesn't release ionizing radiation and displays structures in real-time. Doppler imaging provides details on the hemodynamics of the tissue under investigation. By enabling fast evaluation of several joints in multiple physiological regions in a single session, the US makes follow-up tests for patients rapid, painless, and affordable. With ultrasound, both inflammatory and degenerative RA changes may be observed. High-frequency probes are required to examine the minuscule joints in the hands and feet thoroughly. By utilizing greyscale (B-mode) in ultrasound and doppler techniques, it allows for the assessment of synovitis by iden-

tifying swelling and fluids of the synovial membrane in inflamed joints, bursae, or tendon sheaths as well as by quantifying increased synovial blood flow [4, 21, 35, 50]. The US is extensively used in clinical practice for administering injections and assessing joint inflammation, despite standardization and validation still needing work. However, one of the issues with ultrasound but not MRI is that some areas of the joint may be somewhat inaccessible, such as when investigating the radial and ulnar aspects of the MCP joints. Another primary drawback of ultrasonic detection of erosions is the misreading of typical anatomic abnormalities as erosions. Because the US cannot penetrate bone, its precision for diagnosing bone erosions is location-dependent [51, 59].

2.3.3 X-RAY

Bone erosion, joint space narrowing as an indirect marker of cartilage thinning, osteoporosis, polyps, or cysts, and, in extreme cases, malalignment and ankylosis can all be seen using an X-ray. An X-ray represents the time-integrated cumulative record of joint deterioration. The clinical significance of an X-ray assessment of structural joint damage is determined by its link to a patient-focused outcome, such as how the patient feels, functioning and mobility. These consequences include RA pain and disability. When a disease is established (has been present for over five years), the radiographic damage seen on X-rays is significantly correlated with functional status. It accounts for about 25 percent of the disability. In early disease, X-ray status is not related to functional outcome measures like the Health Assessment Questionnaire (HAQ) score. [[38] One of the significant advantages of an x-ray is it is cost-effective, highly accessible, has reasonable reliability, etc. On the contrary, X-rays have several drawbacks, including ionizing radiation, a lack of sensitivity to early bone damage, projection superimposition caused by the two-dimensional representation of three-dimensional pathology, and an absolute inability to assess soft tissue changes, including synovitis [5, 32, 36, 38].

2.3.4 CT SCAN

High-resolution images of calcified tissue can be seen using the tomographic radiographic imaging technique known as CT. It can be used as a reference standard for identifying the deterioration of calcified tissue, such as bone erosions in RA. Three-dimensional joint viewing is made feasible by multidetector CT with multiplanar reconstruction [1, 38]. The tomographic aspect of CT makes it advantageous. This eliminates the projectional superimposition issue usually seen in X-rays, which potentially masks erosions and simulates joint space narrowing. However, compared to MRI and US, which also employ ionizing radiation, the sensitivity of CT to changes in RA soft tissue is far lower. As a result, CT is rarely used in clinical practice to diagnose RA. Furthermore, the radiation dose of a CT scan of the hand and wrist is similar to conventional X-ray and MRI. As a result, given its limited use in RA diagnosis, many aspects may yet be studied [13, 37, 38].

2.4 EMBEDDED SYSTEMS

Embedded systems are integrated systems with hardware, application software, and a Real-Time Operating system (RTOS) which is reactive and computes in real-time. A typical embedded system has an architecture as can be seen in Figure 2.4, input devices like sensors feed data to an ADC where the real-world analog signals are converted into digital signals. The processors assist in processing the data to determine the output and map it into the memory. A memory usually possesses the ROM where the RTOS is saved and the software is run momentarily. In modern-day systems relying on heavy digital operations for applications ranging from industrial to consumer products to medical devices, embedded systems have become an unparalleled part. Embedded systems can be categorized mainly into three main types: micro-controllers (MCU), Digital Signal Processing (DSP) units, and Field Programmable Gate Array (FPGA) [61].

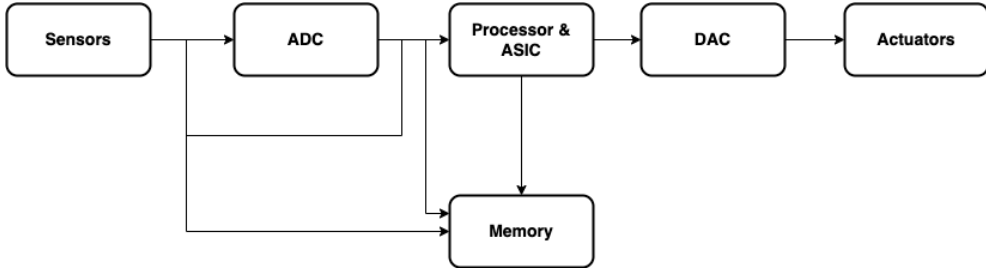


Figure 2.4: Basic Architecture of an Embedded System

DSP unit is a popular option for systems that are designed mainly for the purpose of implementing heavy digital signal processing algorithms like quantization and transformation algorithms. They are widely used in audio signal processing, telecommunications, digital image processing, radar, sonar, and speech recognition systems.^[15] FPGAs fundamentally give the ability to create programmable hardware designs by utilizing an array of programmable blocks with a programmable interconnect. HDL is used to perform designs which are then implemented through RTL synthesis. Contrary to an ASIC, reconfiguration is simple which is merely changing the design and downloading to FPGA platform making it a good choice for prototyping [58].

2.4.1 MICRO-CONTROLLERS

Micro-Controllers are usually small in design and it is often known to serve specific applications. The MCU board consists of a simple microprocessor, peripherals/IO and memory unit like (RAM/EEPROM). An MCU is usually the central part around which an embedded system is built. Micro-controllers are usually categorized based on the number of bits. This data simply represents the ability with what size of data the chip can work on at a time.

2.4.1.1 ARM CORTEX M4

The ARM Cortex M4 processor is a high-performance embedded processor with DSP instructions developed to address digital signal control markets that demand an efficient, easy-to-use blend of control and signal processing capabilities. The processor is highly configurable enabling

a wide range of implementations from those requiring floating point operations, memory protection, and powerful trace technology to cost-sensitive devices requiring minimal area. It achieves exceptional 32-bit performance with low dynamic power, delivering leading system energy efficiency due to integrated software-controlled sleep modes, extensive clock gating, and optional state retention [14].

2.4.2 WIRELESS COMMUNICATION

For electronics engineers and application developers working on Internet of Things (IoT) devices and systems, the connectivity choices are nearly limitless. Because of IoT, the wireless communication industry is quickly evolving. In consequence, communication systems have evolved into a critical component of the IoT infrastructure which connects the gap for bidirectional communication for data gathering and control message delivery. Due to technological advancement, consumers will shift further from PCs and move towards connected devices on the Internet of Things. This will allow consumers to experience real-time and contextual engagement that is no longer impersonal and one-sided. In addition, Messaging will play a significant role in linking not just people to one another, but also applications, and users will also be connected to different IoT devices and sensors. Because of the restricted transmit power, all wireless networks are geographically constrained.

2.5 BLACKBODY TESTING

A hypothetical object that completely absorbs all incident electromagnetic radiation is referred to as a "blackbody." If the temperature of such a body is low enough to prevent self-luminescence, the light does not reflect. This causes them to look black. Any wavelength of radiation is emitted when the blackbody is heated to a specific temperature. In the case of a blackbody, the emissivity (ϵ) and absorptivity (α) are both equal to one.

That is to say

$$\epsilon = 1; \alpha = 1.$$

An ideal blackbody does not retain any of the absorbed energy and emits more energy than any other material at the same temperature. Even though a blackbody is an ideal object, it is possible to construct a radiation source with an emissivity extremely near to that of a blackbody under specific conditions. The energy emitted by a body at a temperature as a function of radiation wavelength over the whole spectrum is given by

$$i(T) = \left(\int_0^{\infty} (\alpha, T) d\alpha \right) (1)$$

It is the radiating body's surface per unit of time, area, and solid angle. The intensity of spectral radiation released by a perfect radiator or blackbody in a vacuum, according to Max Planck's equation of radiation is

$$i_{bb}(\alpha, T) = \left(\frac{2hc^2\lambda^{-5}}{e^{(\frac{hc}{\lambda kT})} - 1} \right) (2)$$

h is Planck's constant, the velocity of light in a vacuum, and Boltzmann's constant. The radiation intensity at all wavelengths is determined by the integration of the entire spectrum⁷.

$$i_{bb}(T) = \frac{2\pi^4}{15h^3c^2}(kT)^4 (3)$$

Lastly, by integrating Eq. (1) throughout the hemispheric space, the emissive power is finally obtained.

$$E_{bb}(T) = \frac{2\pi^5}{15h^3c^2}(kT)^4 = \sigma T^4 (4)$$

which is called the Stefan–Boltzmann's law of radiation and represents the amount of energy emitted hemispherically by a blackbody at temperature per unit of surface area and time and where σ is the Stefan–Boltzmann constant, h is the Planck's constant, the speed of light in vacuum,

and is the Boltzmann's constant. A dimensionless number, also often called the hemispherical total emissivity of the body is defined as the ratio of a real body's emissive power to one of the ideal blackbodies at the same temperature as a real body [33].

$$\epsilon = \frac{E(T)}{E_{bb}(T)} \quad (5)$$

3 | METHODOLOGY

3.1 SYSTEM ARCHITECTURE

The system is designed in a manner where the operations occur in the following sequence shown in 3.1. This is the architecture of the system. Firstly, the device is booted and the lepton goes through the Start-up sequence and waits for around 5000 clock cycles or 200μ seconds. After the initialization, the lepton captures the thermal data of the hand in the FoV, which is 4800 pixels of data per frame. This data is processed and stored in an array by the teensy microcontroller. The data is sent serially to the ESP-12S attached to the teensy. As the data is received in the buffer of the ESP-12S, it serializes the data into a JSON format and transmits it to a connected host database. The image-displaying algorithm fetches the data from the database and displays the image on the PC.

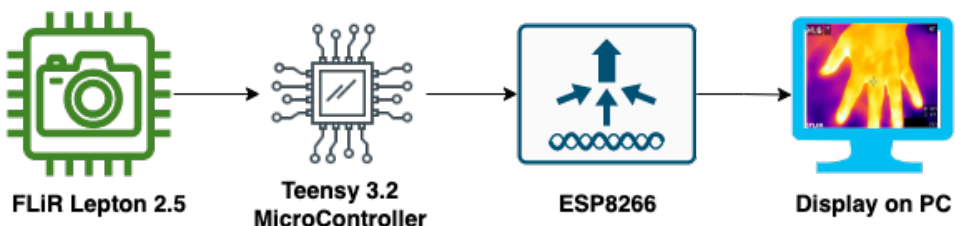


Figure 3.1: System Architecure

3.1.1 SYSTEM FLOWCHART

The first part of the system is devised to acquire images of a hand through the Lepton camera and store it both locally and on the cloud. Figure 3.2 illustrates how a user puts either hand on the Peltier module for it to be heated, and once the temperature is higher than the nearby regions of the hand like the wrist, the user places their hand on the platform where the thermal camera is placed above so that the hand on the platform is covered inside the field of view of the camera. Once an image is captured, it stores the 80 by 60 array image data into a string locally through the SD card and also sends it to be stored as a JSON format on the cloud database through WiFi shield. This stored data is then used with image processing tools, to be displayed on the PC.

The state diagram of the full system design is presented in Figure 3.3. Here we present the processes in a more detailed manner. The system begins when there is an external signal through the GPIO of the teensy which turns the Peltier module ON. Once the temperature reaches the steady state temperature, it checks if there is any hand placed on the hand warming platform. As the hand warms up, a second GPIO sends out a signal for 3 images to be taken where there is no hand in the FoV. Then the user puts their hand on the image capturing platform where 10 images are captured in the time span of 30 seconds. These images are then stored locally and uploaded to the cloud database. Then the next hand is asked to be placed on the device and the same flow is followed for the second hand.

Due to the time limitations and constraints, we focus on the first part of the system where we develop the image capturing system which can be further analyzed to understand if thermo-graphic images are beneficial in the diagnosis of RA.

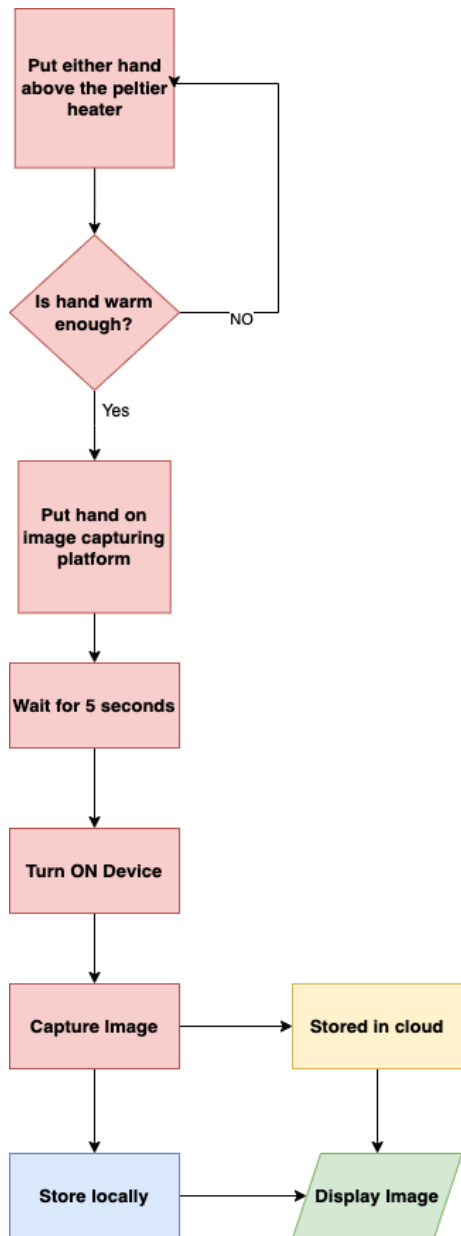


Figure 3.2: Data collection phase system flowchart

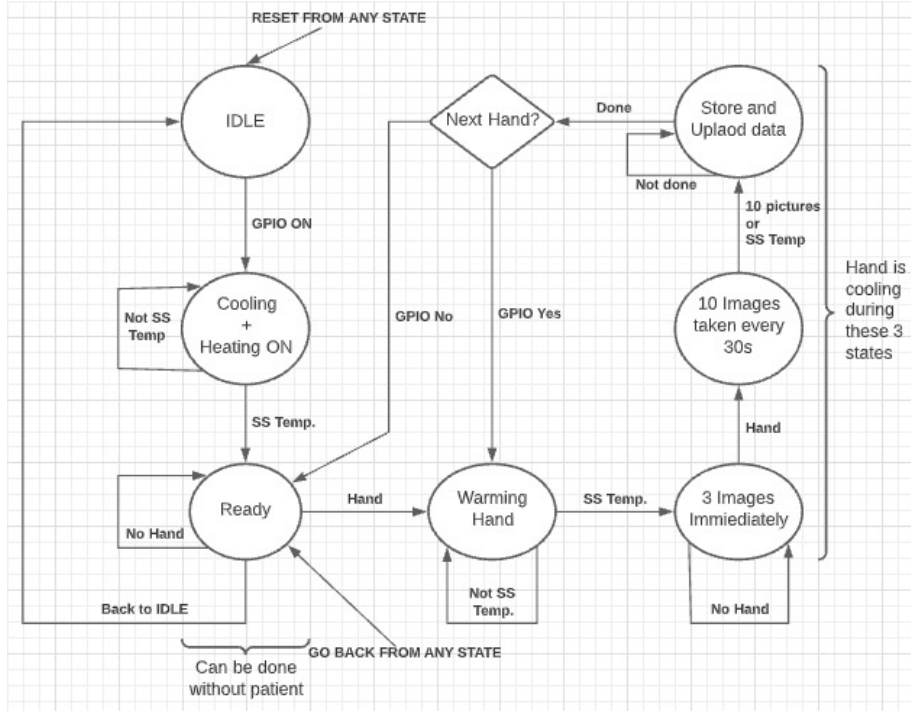


Figure 3.3: Full system flowchart

3.1.2 FLIR LEPTON IMAGE CHARACTERISTICS

The generic VoSPI packet possesses a 4-byte header which is accompanied by either a 160-byte or 240-byte payload as shown in Figure 3.4. In our case, we define each VoSPI frame to be of size 164-byte. This VoSPI frame that is transferred through high throughput, 20MHz SPI channel is the image we want to acquire. All the data from the 60 rows of the sensor are transferred to the MCU through this frame.

The header has a 2-byte ID and a 2-byte CRC. ID is a 12-bit packet numbering for all the packets sent from lepton. This packet numbering is reset for each new frame sent so the next frame starts numbering from zero. The CRC is a 16-bit cyclic redundancy check(CRC), which is computed using the following polynomial:

$$x^{16} + x^{12} + x^5 + x^0$$

If the host (Teensy) finds a discrepancy after calculating the CRC, it re-synchronizes the VoSPI

ID	CRC	Payload
4 bytes		160 or 240 bytes (depending upon bit resolution setting)

Figure 3.4: FLiR Lepton 2.5 and Teensy 3.2 Schematic

Byte 0	Byte 1	Byte 2	Byte 3	...	Byte 158	Byte 159
Line m Pixel 0		Line m Pixel 1		...	Line m Pixel 79	

Figure 3.5: 1 video line per 160-byte payload

stream to avoid potential misalignment.

For each SPI transaction, Lepton sends VoSPI packets consisting of data of

$$\text{Each Payload} = 80 \text{pixels} \times 2 \text{bytes/pixel} = 160 \text{bytes/Payload} \text{ (Figure 3.5)}$$

$$160 \text{bytesPayload} + 4 \text{bytesHeader} = 164 \text{bytes/Videopacket}$$

$$\text{Each frame/image} = 60 \text{Videopacket}$$

$$\text{Total bytes for a 60pixel of data} = 164 \text{bytes/Videopacket} \times 60 = 9840 \text{ bytes/image (3.6)}$$

Telemetry mode	Header		Payload
	ID	CRC	
Packet 0	2Bytes	2Bytes	160Bytes
Packet 1	2Bytes	2Bytes	160Bytes
Packet 2	2Bytes	2Bytes	160Bytes
Packet 3	2Bytes	2Bytes	160Bytes
...
Packet 29	2Bytes	2Bytes	160Bytes
Packet 30	2Bytes	2Bytes	160Bytes
Packet 31	2Bytes	2Bytes	160Bytes
Packet 32	2Bytes	2Bytes	160Bytes
...
Packet 58	2Bytes	2Bytes	160Bytes
Packet 59	2Bytes	2Bytes	160Bytes

Figure 3.6: Video Packet Contents Per Frame

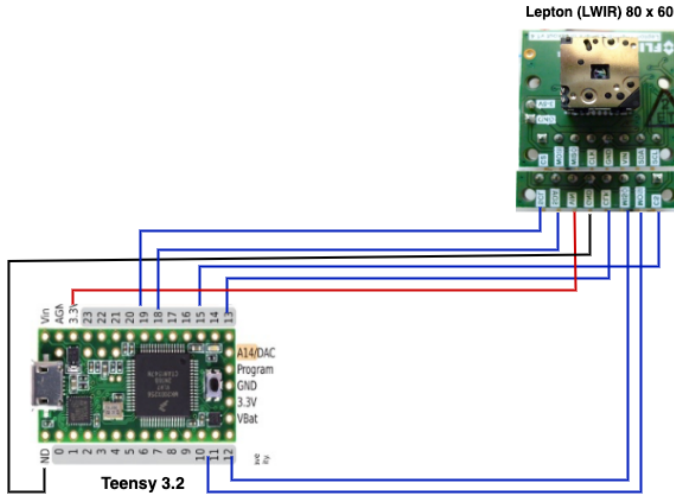


Figure 3.7: FLiR Lepton 2.5 and Teensy 3.2 Schematic

3.2 IMAGE ANALYSIS TECHNIQUE

3.2.1 LEPTON RAW DATA TO THERMAL IMAGE

The steps followed from receiving raw data from the thermal camera to a proper thermal image is described in [3.8](#). First, the raw data from the thermal camera is captured and converted into a 2D array of temperature values. The resulting temperature values are then normalized using a min-max normalization, which scales the values to a scale of 0 to 1. This normalization step can help to make the image more visually appealing and easier to interpret.

Next, a colormap is chosen and used to map the normalized temperature values to a specific set of colors. A color map is a function that assigns a specific color to each temperature value, with different colormaps producing different visual effects. The colored values are then used to create a 2D temperature image, with each element in the image corresponding to a pixel in the final image.

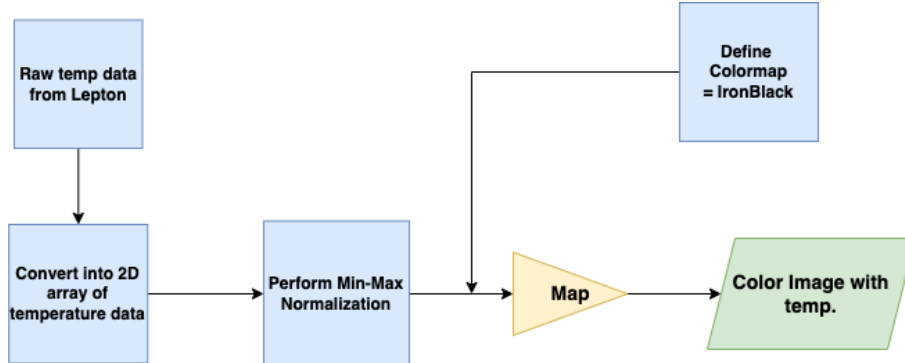


Figure 3.8: Flow of Thermal Image Conversion

3.2.2 THERMAL COLOR IMAGE TO THERMAL GRayscale IMAGE

Each of the color channels is converted to grayscale. The luminance of each pixel is calculated using the following formula:

$$gray = 0.299 * red + 0.587 * green + 0.114 * blue$$

This formula weights the contribution of each color channel based on how the human eye perceives color [12]. The grayscale channels are combined into a single grayscale image. Once all of the color channels have been converted to grayscale, they can be combined into a single image by replacing the red, green, and blue channels with the corresponding grayscale values. Then we scale the indexed grayscaled image so that its actual temperature in degC can be output instead of grayscale indexes.

3.3 SYSTEM COMPONENTS

Here, all the singular components integrated into the system are discussed in detail in terms of their specifications, justifications of choice over the alternatives, and their role in the system.

Dimensions (mm)	8.5 x 11.7 x 5.6
Thermal sensitivity (mK)	<50
HFOV (\circ)	51
Resolution (pixel)	60x80
Frame rate (Hz)	9
Scene Dynamic range ($^{\circ}$ C)	-10 to +140
Communication interface	SPI
Current consumption (mA)	100
Price(\$)	210

Table 3.1: Key Specifications of Lepton 2.5

3.3.1 FLIR LEPTON 2.5

FLIR Lepton 2.5 used in this system, is a long-wave infrared-based microbolometer sensor array with an 80x60 resolution camera system from Teledyne FLIR which comes with a socket configuration that can be directly integrated with Lepton thermal camera breakout board. It comes with an integral shutter assembly that enables optimized image uniformity on a periodic basis. It has a frame rate of 9Hz and is capable of capturing a temperature range of -10 to +140°C. It is a great option for applications requiring very low power that require an instant-on operation. The key specifications are noted in [3.1](#)

3.3.2 TEENSY 3.2

Teensy 3.2 is a low-power, tiny-sized ARM Cortex-M4-based microcontroller from PJRC solutions. It is compatible with Arduino software and libraries which makes the implementation with

Clock Speed (MHz)	72
Flash Memory (kB)	256
RAM (kB)	64
Digital I/O	34
General Purpose DMA Channels	34
Price(\$)	22

Table 3.2: Key Specifications of Teensy 3.2 [43]

Teensy very versatile. It has RTC for date/time, 23 Digital I/O pins, 21 Analog Input pins, and most importantly 3 serial, 1 SPI, and 2 I2C ports with the flexibility of adding memory options like SD card through SPI lines, as stated in 3.2, making it a very suitable choice for the proposed device [43]. The relatively cheaper price of the teensy also makes it a good option for this application compared to other microcontrollers. Teensy is used as the main brain of this system. It interfaces with both lepton thermal camera and the ESP-12S WiFi shield and acts as the middle layer between the both.

3.3.3 ESP12-S

Ai-Thinker Technology developed the ESP-12S WiFi module. The industry-leading Tensilica L106 ultra-low-power 32-bit micro MCU is integrated into the core processor of the ESP8266. It is clocked at 80 MHz and 160 MHz, supports RTOS, and integrates Wi-Fi MAC and has a SPI flash of 32 MBit with an average power consumption of 71mA during continuous transmission at a baud rate of 115200 bits per second [54]. Table 3.3 summarizes the key specifications of ESP-12S. This WiFi module is included in the system for giving it the ability to send the image data to a host which is wirelessly connected through the WiFi.

Dimension (mm)	24x16x3(± 0.2)
Flash Memory (MBit)	32
UART Baud rate	Default 115200 bps
Frequency Range(MHz)	2412 to 2484
Power (mA)	Average ~ 71
Price(\$)	5.0

Table 3.3: Key Specifications of ESP-12S [54]

3.3.4 PELTIER MODULE

Thermoelectric modules (TEC) or peltier, are a type of heat pump that is powered by electricity. Here, heat-based energy must be dissipated after being transmitted from one side of the module to the other. The so-called Peltier effect, which describes the quasi-inverse of the Seebeck effect, is the foundation of the Peltier module. According to the Peltier effect, a temperature difference caused by a current flow in a semiconductor can convey energy in the form of heat. The Seebeck effect also explains how inducing a temperature differential, a semiconductor experiences a current flow[57]. The advantage of Peltier lies in its ability of reversal of heat flow through the negation of the polarity and precise control. The peltier module is used with an aluminum plate attached on top which works as the platform for the user to warm or cool their hands. The specifications are shown in 3.4.

Module dimension(mm)	40 x 40
Al plate dimension(mm)	40 x 60
Weight(g)	455
Wattage	60W nominal (12V * 5A), 72W max

Table 3.4: Key Specifications of Peltier Module [57]

3.4 SYSTEM DESIGN AND IMPLEMENTATION

We know from previous parts that the system is mainly based on three main components:

1. LWIR camera: FLiR Lepton
2. ARM-Cortex M4 micro-controller: Teensy 3.2
3. IEE802.11 wireless module: ESP-12S

In this part, we will explain how these components are designed and implemented collaboratively in devising the developed system.

3.4.1 PHYSICAL CONNECTION

There are two different physical connection configurations used in this system. First, direct connections between the Teensy microcontroller and the Lepton camera. The connected pins are tabulated in 3.5. The Lepton thermal camera breakout board v1.4 has 8 pins. The schematic in Figure 3.7 portrays how it is connected to the Teensy. The connected pin are power pins, SPI and I^2C communication pins.

On the other hand, Table 3.6 shows all the connected pins between the Teensy to the ESP-12S module. The two modules are connected physically in this manner shown in Figure 3.9.

Lepton 2.5	Teensy3.2
I^2C SCL	PIN 19
I^2C SDA	PIN 18
SPI CS	PIN 2
SPI MOSI	PIN 11-DOUT
SPI MISO	PIN 12-DOUT
SPI CLK	PIN 13
GND	GND
VIN	+3.3V(100mA max)

Table 3.5: Physical pin connection (Lepton-Teensy)

ESP-12S	Teensy3.2
TXD0	TTL-RXD3
RXD0	TTL-TXD3
ESP-GPIO15	GND
ESP-GPIO2	+3.3V
ESP-GPIO0	+3.3V
VCC	+3.3V
ESP-RST	+3.3V
ESP-CH-PD	+3.3V

Table 3.6: Physical pin connection (ESP-Teensy)



Figure 3.9: Physical connection between Teensy and ESP shield

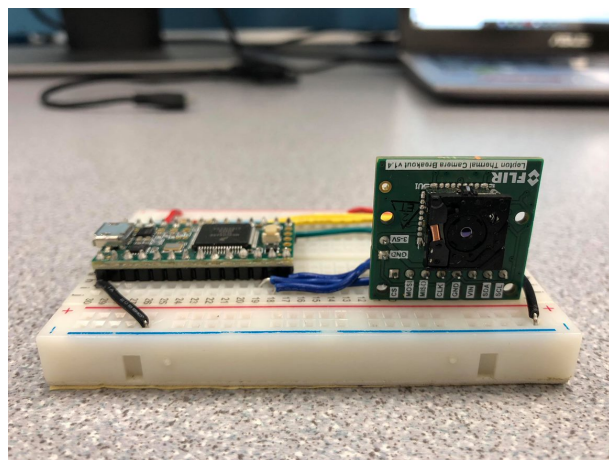


Figure 3.10: Physical connection between Teensy and Lepton

3.4.2 IMPLEMENTATION OF SERIAL COMMUNICATION (FLIR LEPTON - LEPTON3.2)

There are two subsequent serial communications that take place between Lepton and Teensy during any image capturing operation. Lepton has a I2C-like two-wire interface called command and control interface (CCI). Contrary to two conventional I2C standards, CCI is only capable of 16-bit transfers since all lepton registers are 16 bits wide. The CCI address stated in the datasheet is 0x2A. In general, the commands executed through the CCI are in the form of "get" for reading data, "set" for writing data or "run" to execute any desired function [18]. Commands like Flat Field Correction (FFC) for re-calibration, and Automatic Gain Control (AGC) are used for converting the dynamic range of data to a more suitable rate for a display. For lepton, it is 14-bit to 8-bit. The other specialized communication known as VoSPI (Video over Serial Peripheral Interface) is utilized for transferring 60 packets per frame. The VoSPI includes 3 lines of a typical SPI channel: Chip Select (CS), SCLK (Slave Clock), MISO (Master-in Slave-out). The MOSI (Master-out Slave-in) is not utilized in this design, so it is set to low in our configuration as illustrated in 3.11. VoSPI is packet-based and does not require flow control or embedded timing signals. The implementation of this communication is allocated for single master (Teensy 3.2) and a single slave (FLiR lepton 2.5). The Teensy determines the clock speed and executes all sorts of transactions from the Lepton camera. 3.12 shows the SPI Mode 3 (CPOL = 1, CPHA = 1) used during this SPI communication, which denotes to when the communication is idle, the SCK (clock) signal is HIGH. This mode basically sets up the data from Lepton during the falling edge of the clock (SCK) and sequentially, the data is sampled by Teensy on the rising edge. Data from the slave out to master is transmitted in big-endian order with the most-significant byte first.

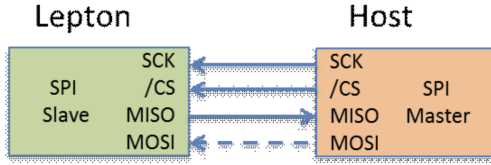


Figure 3.11: SPI communication: Lepton and Host (Teensy) [18]

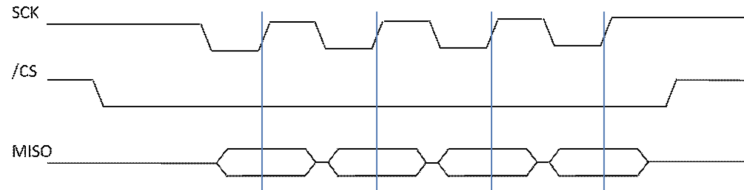


Figure 3.12: Illustration of SPI Mode 3[18]

3.5 DATA ACQUISITION

3.5.1 SPI COMMUNICATION: TEENSY AND LEPTON

Defining the data acquisition model is a vital part of this project. The SPI communication is initiated from the Teensy MCU, whenever it demands data from the Lepton. In order to enable SPI communication, the clock is configured at the maximum frequency of 20 MHz. The CS pin is then put to LOW state, which begins a communication channel with the Lepton camera. Internal shift registers are used to transfer the data in sizes of 8-bit. MCU shifts register value out through the MOSI line, and the camera shifts data into its shift register. Data are shifted out with the MSB first while shifting a new LSB into the same register. Once the data in the register has been shifted out, the MCU and the camera have exchanged their register values, the MCU puts the data received from the camera into a buffer (RxBuffer). This above flow is shown in Figure 3.13.

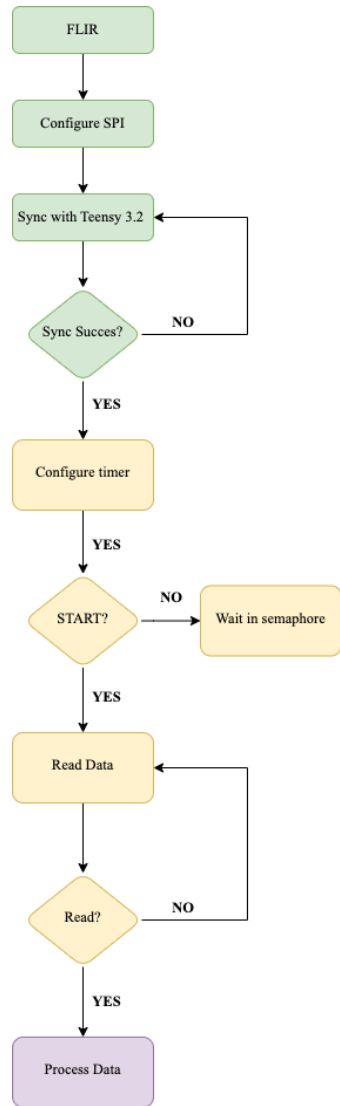


Figure 3.13: Data acquisition model

3.5.2 SERIAL COMMUNICATION: TEENSY AND ESP-12S

The sequential procedure of the communication between the MCU and WiFi module is illustrated in Figure 3.14. Initially, the ESP module instantiates a Universal asynchronous receiver-transmitter (UART) Serial communication port at a baud rate of 115200 bits per second. It then connects to a WiFi AP (Access Point). Once it is connected to the WiFi AP, it waits to receive any data from the Teensy. A pointer is initiated in the Rx buffer and is iterated for $i_t h$ element, the Teensy also flushes the serial buffer to remove any remaining data from previous communications. The first LSB is sent through to the Read buffer of the ESP, which also clears the buffer before any data is received. Once received, the ESP sends an ACK signal, acknowledging that it received the last byte Teensy transmitted. Once the ACK is received, the ESP realizes it needs to transmit the MSB of the $i_t h$ element to the Teensy. Once the MSB is received the ESP sends an ACK(@) through UART back to the Teensy. This process continues until all the elements in the array is transmitted. During this process, if any ACK is not received within a span of 30 seconds the user is reported that there is a possible connection lost.

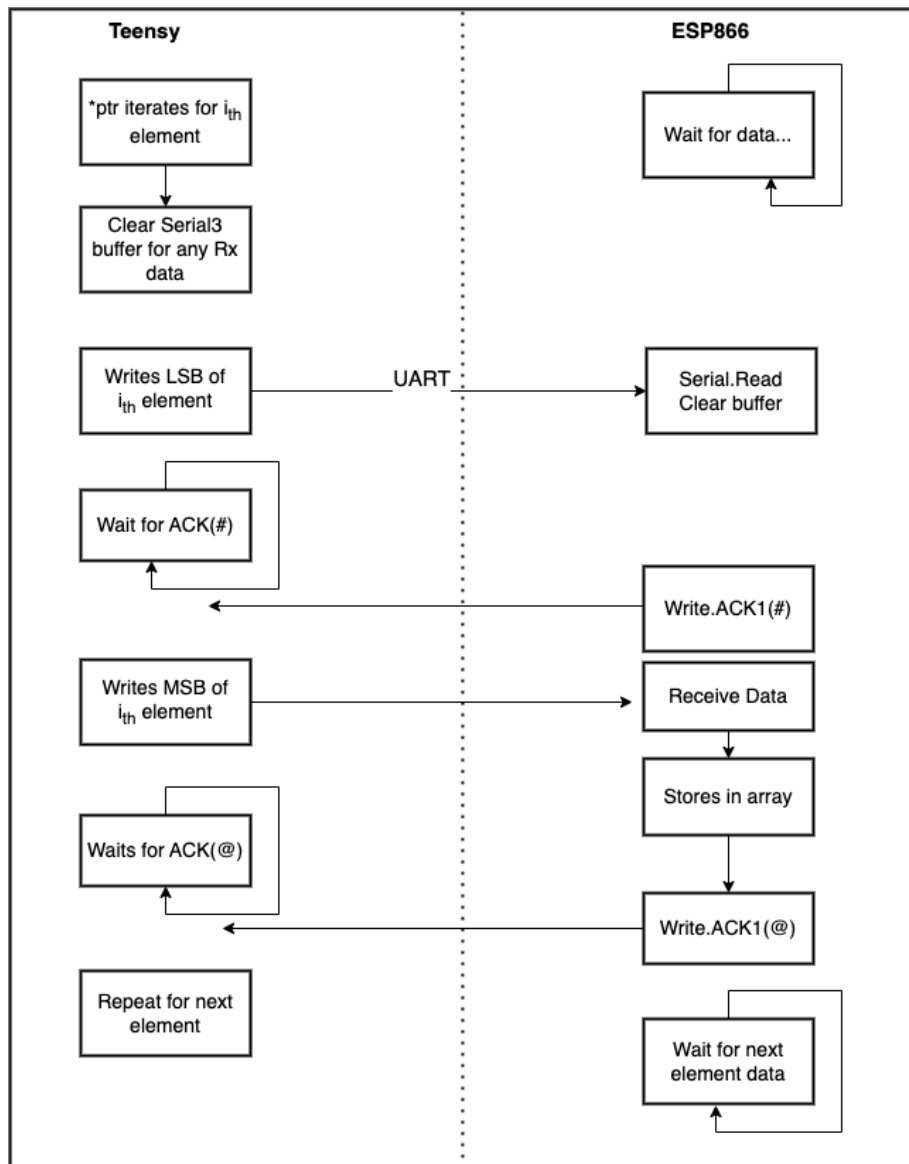


Figure 3.14: Communication between Teensy and ESP shield

4 | RESULTS AND DISCUSSION

In this chapter, the developed system and the initial results are evaluated and presented.

4.1 INITIAL EXPERIMENTS

The initial setup was tested by capturing images of the hand of a healthy individual at different orientations. Six different orientations are represented with their thermal image with a defined colormap whose rgbmap is shown in 4.3, the original image, a grayscale image based on min values, along with a grayscale image with the minimum and maximum temperature range.

The initial images were processed by the default rgb colormap which outputs the images with higher mean absolute error (MAE) and is not beneficial in understanding any information of the hand. The first image in 4.1 shows an absolute noisy background when there is no object in the Field of View (FoV). The image in 4.2 shows an uninformative, wrongly scaled thermal image when default colormap was used.

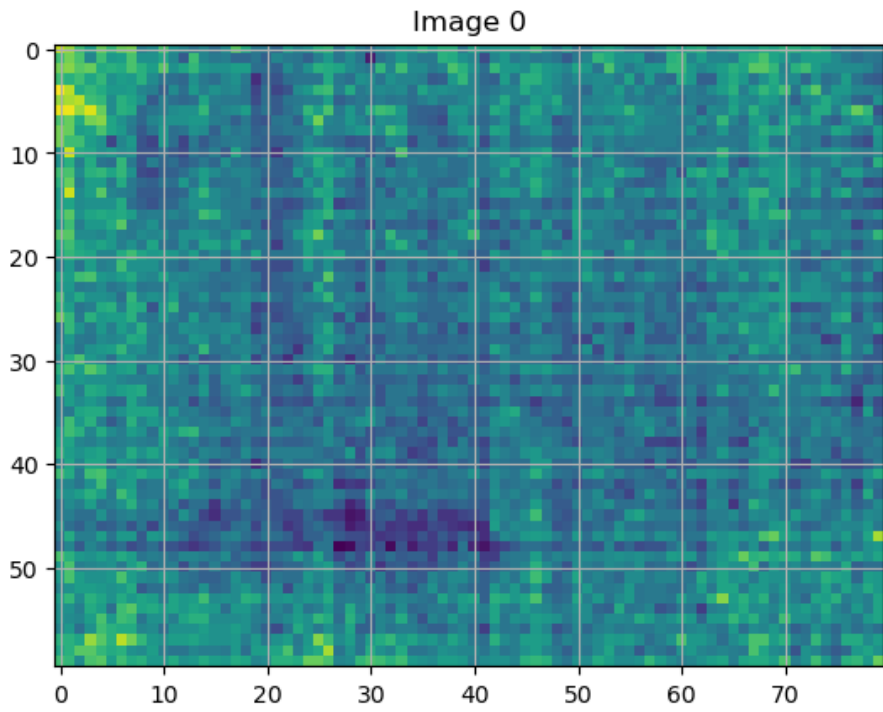


Figure 4.1: Image of noisy background

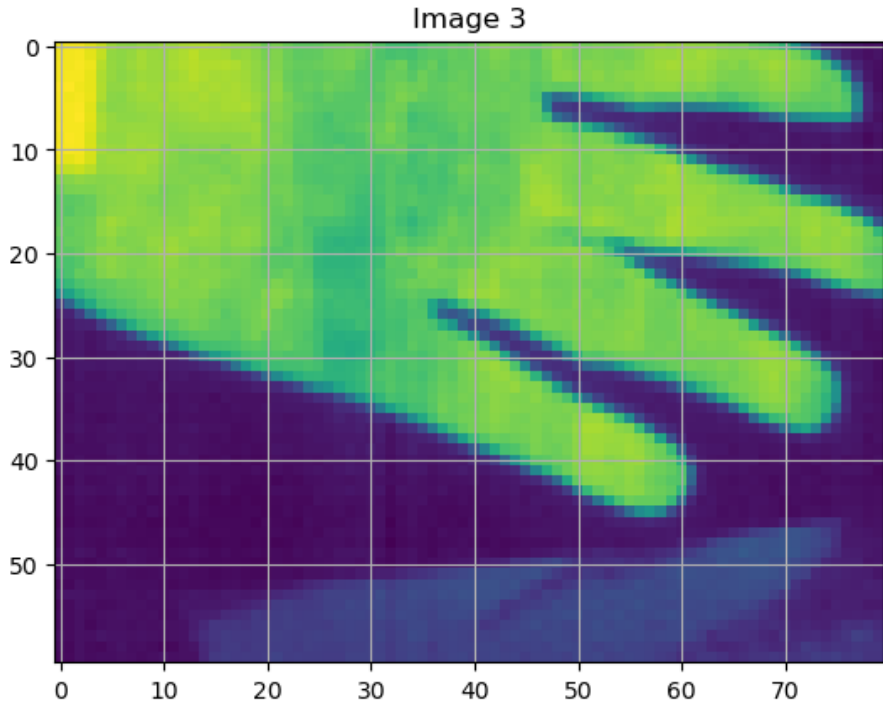


Figure 4.2: Image from default colormap

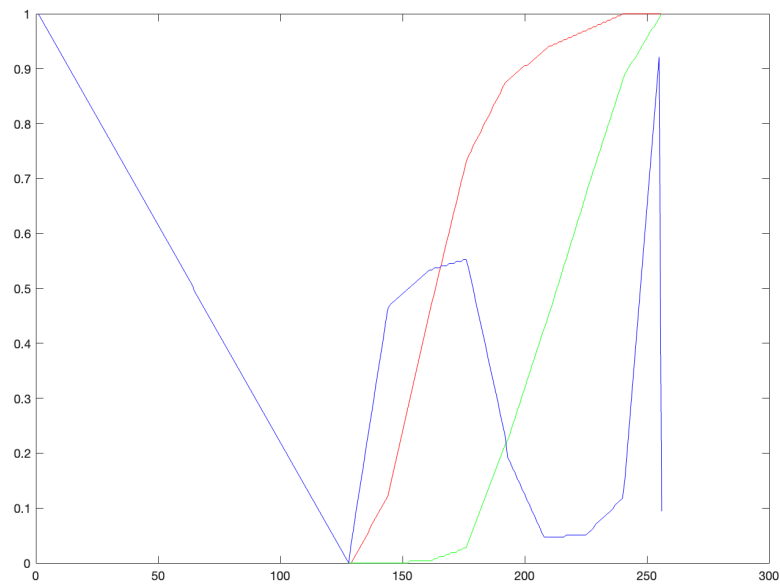


Figure 4.3: RGB Plot of the Colormap used

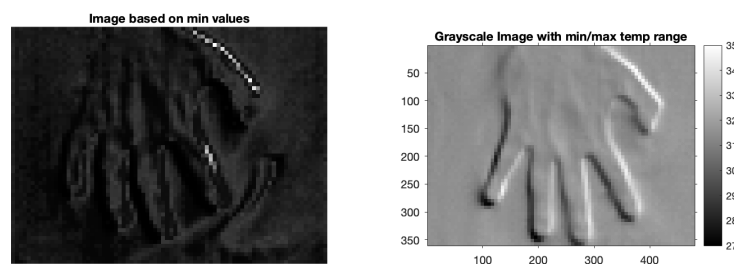
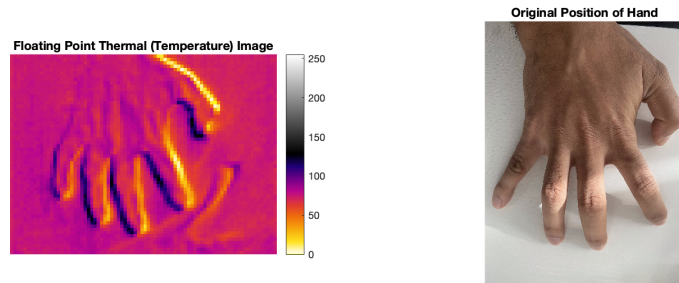


Figure 4.4: Hand Position 1

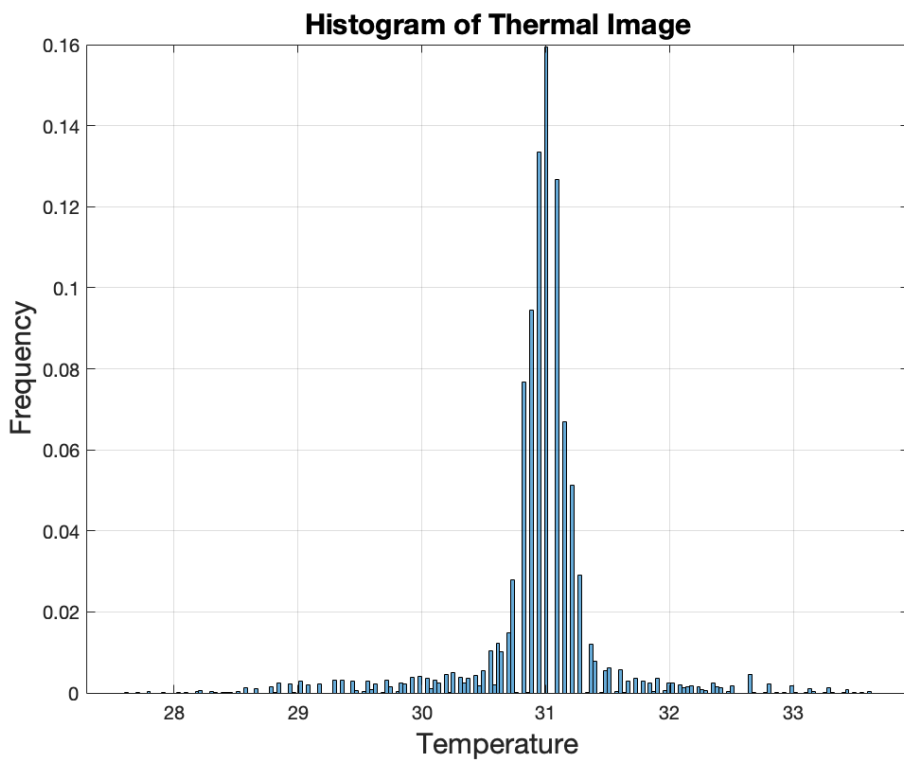


Figure 4.5: Histogram of thermal image in position 1

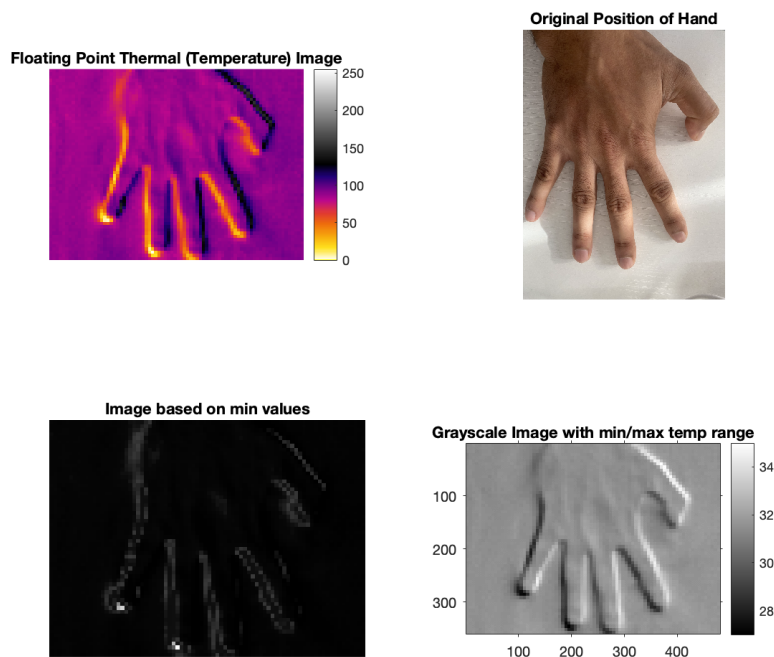


Figure 4.6: Hand Position 2

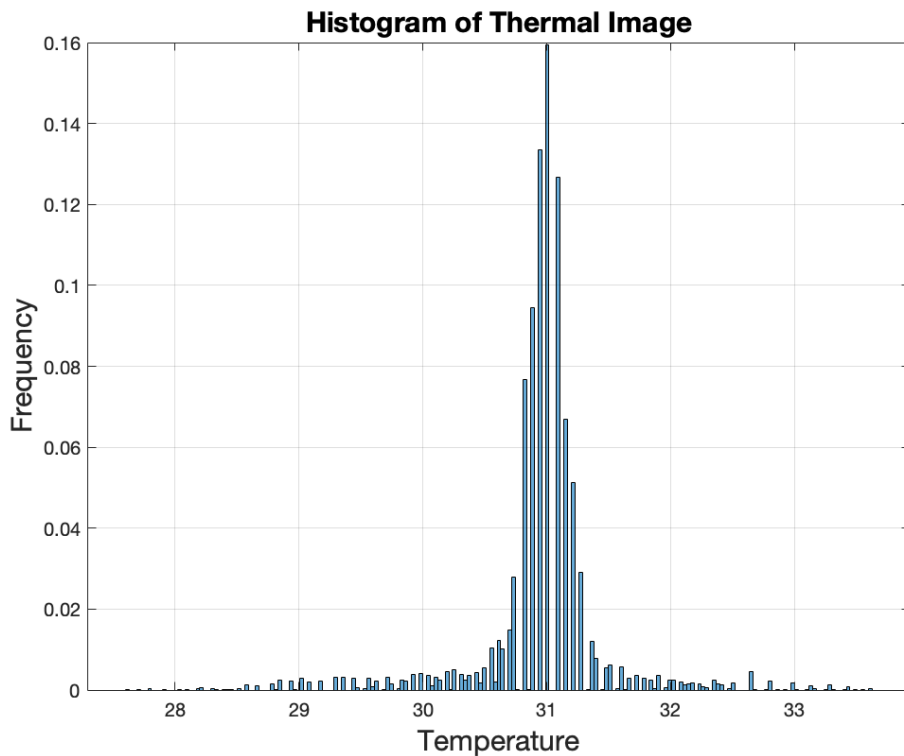


Figure 4.7: Histogram of thermal image in position 2

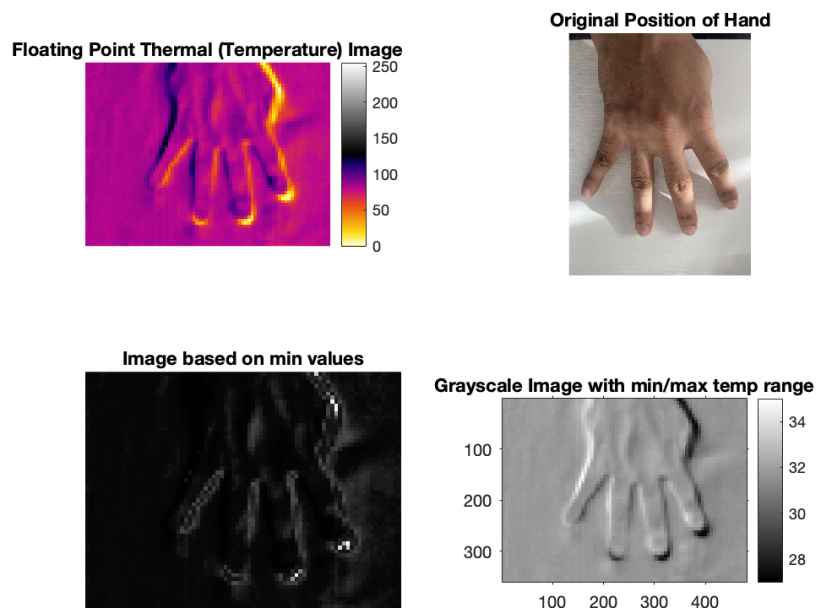


Figure 4.8: Hand Position 3

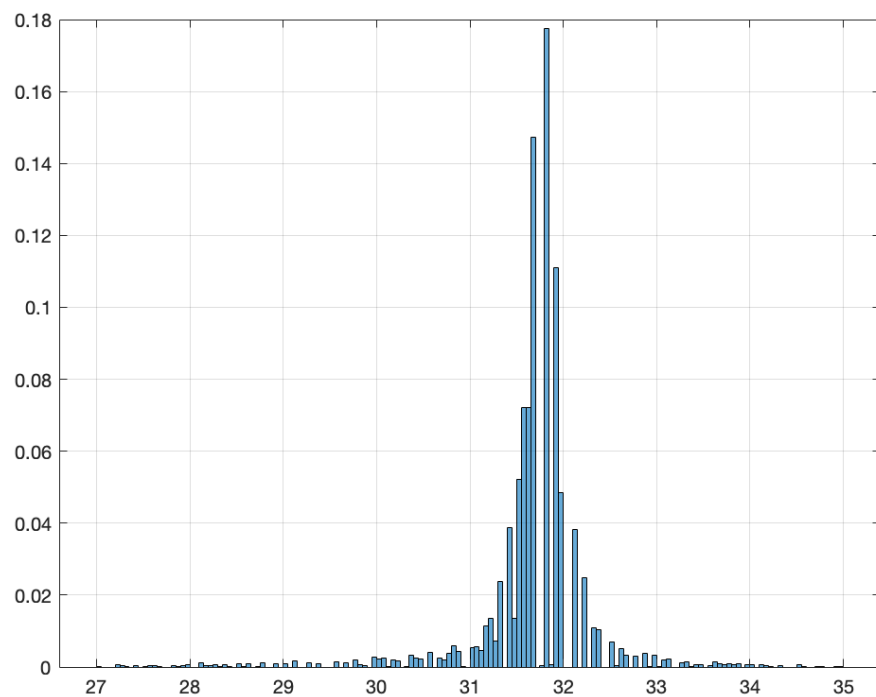


Figure 4.9: Histogram of thermal image in position 3

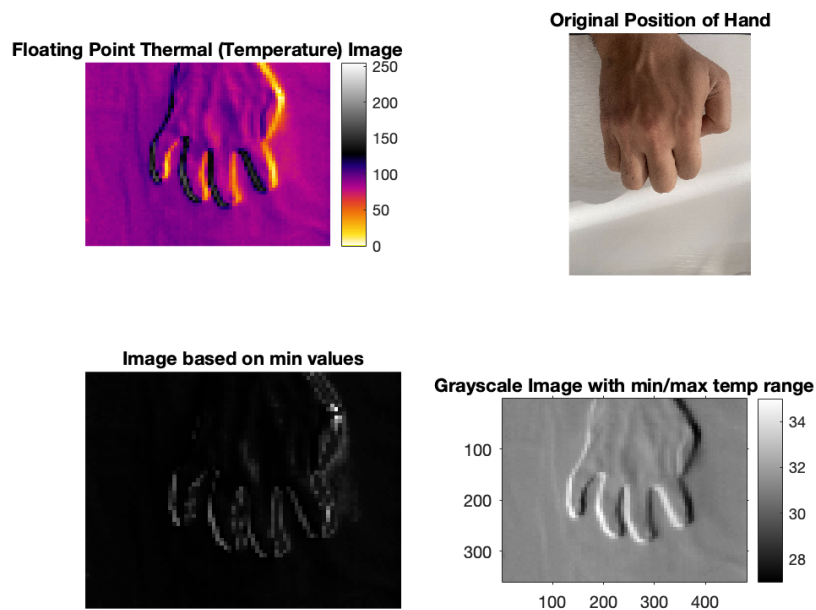


Figure 4.10: Hand Position 4

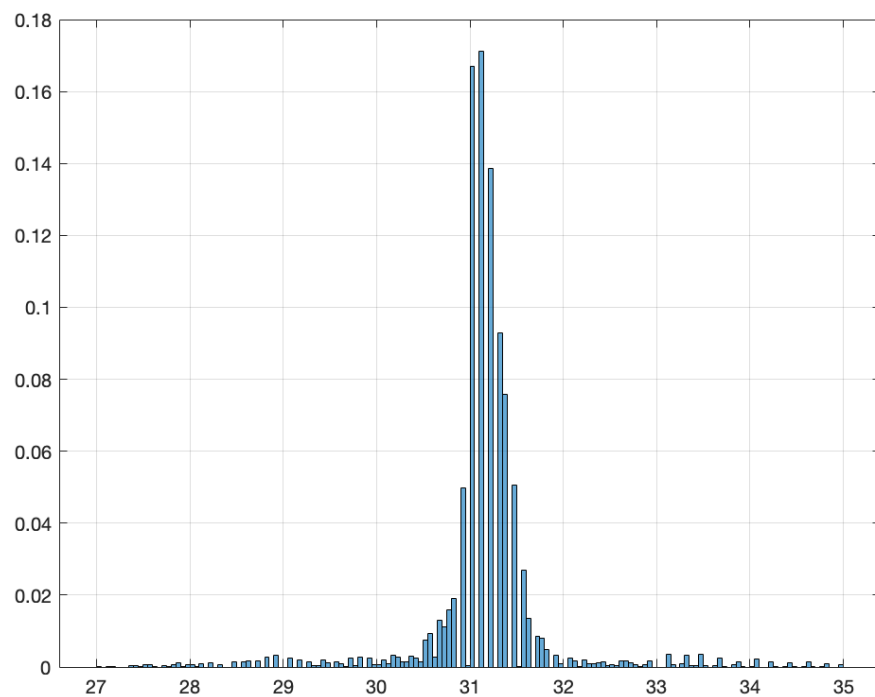


Figure 4.11: Histogram of thermal image in position 4

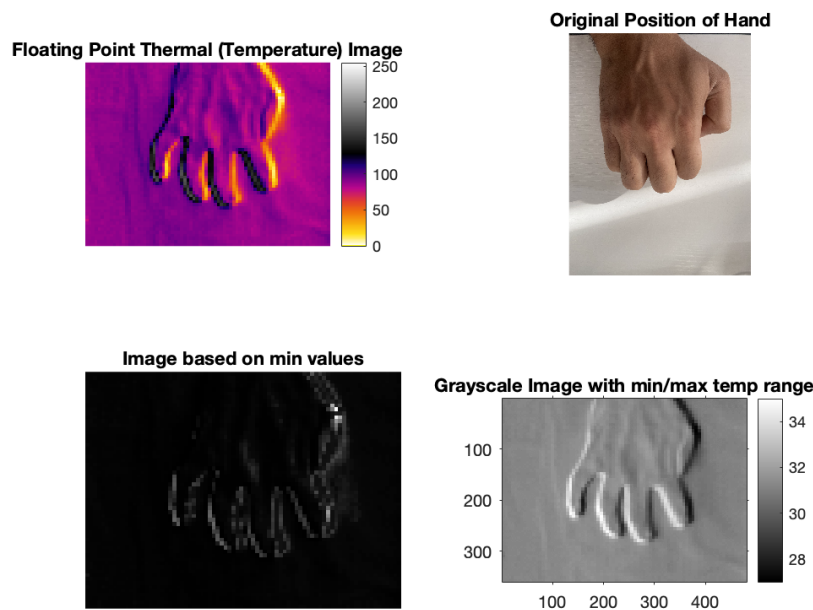


Figure 4.12: Hand Position 5

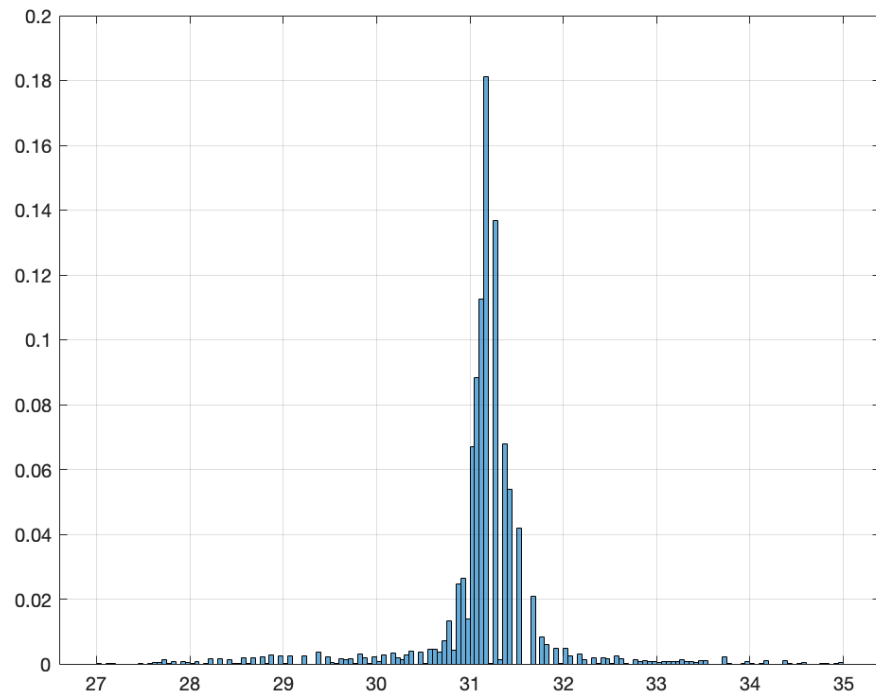


Figure 4.13: Histogram of thermal image in position 5

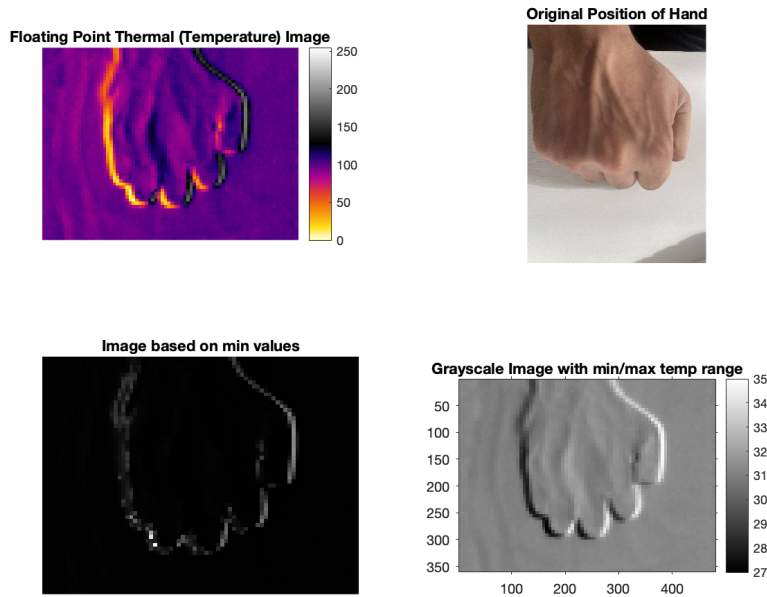


Figure 4.14: Hand Position 6

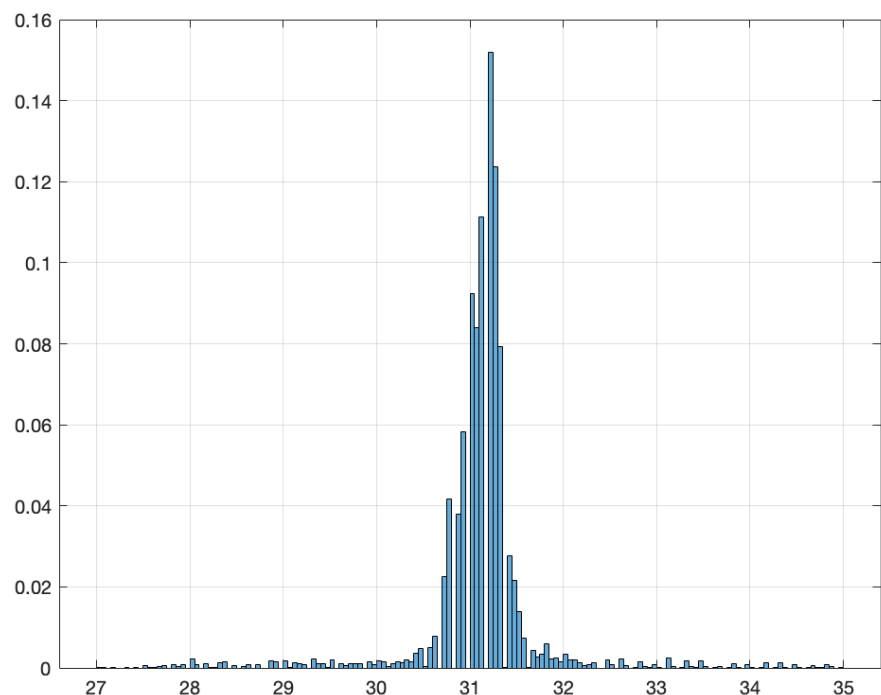


Figure 4.15: Histogram of thermal image in position 6

4.2 DISCUSSION

The results are displayed in a manner where the first figure is the thermographic image after the colormap was initiated. The second figure displays the real image of the configuration of the hand which helps in understanding the orientation of the hand for which achieving an optimal thermal image might be challenging. The third figure shows images that are calculated based on the min elements of the original RBG image data array. It is useful for finding different regions of an image. The final image portrays the grayscale image of the thermal image which is scaled by the lowest temperature and the difference between the highest and lowest temperature so that its actual temperatures in °C can be observed rather than in grayscale indexes. There are six different hand orientation that depicts different possibilities of hand deformities in RA patients. It can be seen that there is a visible difference in the areas near the fingers compared to the other areas of the hand. The histogram for all the hand positions shows a similar characteristic where the maximum temperature is around 31-33°C, which is the average temperature of the human hand. In the output images, we can observe that image taken at position 6 shown in Figure 4.14 might not be suitable since it shows the least contrast between the knuckle and the surrounding areas. The image at position 1 shows poor contrast in temperature which makes the minimum element figure to be absolutely unusable. Images are shown in Figures 4.6, 4.8, 4.12 show that from the output images, we can acquire acceptable distribution in the histogram which provides the quantifiable contrast in temperature between the Region of Interest (ROI) and other parts of the hand. Since the scene is essentially stationary, images were taken after Flat Field Correction (FFC) process is executed. This allows the camera to recalibrate any drift that occurred during the process maintaining satisfactory uniformity. As the images are compared we can see the images taken subsequently are independent of each other.

5 | CONCLUSION AND FUTURE WORKS

5.1 PROJECT OVERVIEW

The outmost goal for this thesis was to develop a system that is low-cost, non-invasive and small in size for the application of diagnosing of Rheumatoid Arthritis. This was achieved through integrating the thermal camera with an embedded device, the communication interface was also defined and performed for the system to have the connectivity abilities to send data packets through the WiFi or Internet. In this thesis, we presented the design and prototype of an end-to-end functional thermal image acquisition and display system which enables thermal image acquisition and display of human hand and using specified colormap. All the image analysis were done in MATLAB R2020b version. We explored the application for Infrared thermal camera for detecting temperature variation between human hand and background. It was observed through simple histogram distribution that more temperature magnitude observed on the Region of Interest. The images show a reliable indication for the functionality of the thermal camera system to provide detailed image of human body temperature's distribution.

5.2 FUTURE WORK

Future scope for this work lies in the study of knuckle detection and segmentation from the thermal images of hand. A model based on convolutional neural networks (CNN) that is trained

in variety of configurations and environmental conditions can be valuable in the development of the feature selection and classification model as suggested by researchers [7], [31]. Part of the success of the model depends on the achievement on high quality image data from both healthy individuals and RA patients that can be collected over a period of time.

BIBLIOGRAPHY

- [1] Eeva Alasaarela et al. “Evaluation of humeral head erosions in rheumatoid arthritis: a comparison of ultrasonography, magnetic resonance imaging, computed tomography and plain radiography”. In: *British journal of rheumatology* 37.11 (1998), pp. 1152–1156. ISSN: 1462-0332.
- [2] Frank C Arnett et al. “The American Rheumatism Association 1987 revised criteria for the classification of rheumatoid arthritis”. In: *Arthritis Rheumatism: Official Journal of the American College of Rheumatology* 31.3 (1988), pp. 315–324. ISSN: 0004-3591.
- [3] MA Aweda et al. “Potential role of thermography in cancer management”. In: *Arch Appl Sci Res* 2.6 (2010), pp. 300–12.
- [4] et al. Backhaus M. “Arthritis of the finger joints: a comprehensive approach comparing conventional radiography, scintigraphy, ultrasound, and contrast-enhanced magnetic resonance imaging.” In: *Arthritis Rheumatism: Official Journal of the American College of Rheumatology* 42.6 (1999), pp. 1232–1245.
- [5] M Backhaus et al. “Prospective two year follow up study comparing novel and conventional imaging procedures in patients with arthritic finger joints”. In: *Annals of the rheumatic diseases* 61.10 (2002), pp. 895–904. ISSN: 0003-4967.

- [6] Subramnaiam Bagavathiappan et al. "Correlation between plantar foot temperature and diabetic neuropathy: a case study by using an infrared thermal imaging technique". In: *Journal of diabetes science and technology* 4.6 (2010), pp. 1386–1392.
- [7] Ewelina Bartuzi et al. "Unconstrained biometric recognition based on thermal hand images". In: June 2018, pp. 1–8. doi: [10.1109/IWBF.2018.8401567](https://doi.org/10.1109/IWBF.2018.8401567).
- [8] N Benton et al. "MRI of the wrist in early rheumatoid arthritis can be used to predict functional outcome at 6 years". In: *Annals of the Rheumatic Diseases* 63.5 (2004), pp. 555–561. ISSN: 0003-4967.
- [9] NIKOLA BOROJEVIĆ et al. "Thermography hand temperature distribution in rheumatoid arthritis and osteoarthritis". In: *Periodicum biologorum* 113.4 (2011), pp. 445–448.
- [10] Kunlin Cao et al. "Toward Quantitative Assessment of Rheumatoid Arthritis Using Volumetric Ultrasound". In: *IEEE Transactions on Biomedical Engineering* 63.2 (2016), pp. 449–458. doi: [10.1109/TBME.2015.2463711](https://doi.org/10.1109/TBME.2015.2463711).
- [11] A Capo et al. "Joint functional impairment and thermal alterations in patients with Psoriatic Arthritis: A thermal imaging study". In: *Microvascular Research* 102 (2015), pp. 86–91.
- [12] Saravanan Chandran. "Color Image to Grayscale Image Conversion". In: (Apr. 2010), pp. 196–199. doi: [10.1109/ICCEA.2010.192](https://doi.org/10.1109/ICCEA.2010.192).
- [13] Philip G Conaghan et al. "The validity and predictive value of magnetic resonance imaging erosions in rheumatoid arthritis: Comment on the article by Goldbach-Mansky et al". In: *Arthritis Rheumatism* 50.3 (2004), pp. 1009–1011. ISSN: 0004-3591.
- [14] "Cortex M4 Devices: User Guide". In: (2011).
- [15] D.Stanzione. *Dsp architectural innovation: John thompson's technique*. Vol. 9. 1. 2017, pp. 19–20. doi: [10.1016/j.proeng.2015.08.784](https://doi.org/10.1016/j.proeng.2015.08.784).

- [16] Uffe Døhn et al. “Are bone erosions detected by magnetic resonance imaging and ultrasonography true erosions? A comparison with computed tomography in rheumatoid arthritis metacarpophalangeal joints”. In: *Arthritis research therapy* 8 (Feb. 2006), R110. doi: [10.1186/ar1995](https://doi.org/10.1186/ar1995).
- [17] Michael Elßner and Holger Vogt. “Reliability of Microbolometer Thermal Imager Sensors Using Chip-scale Packaging”. In: *Procedia Engineering* 120 (Dec. 2015), pp. 1191–1196. doi: [10.1016/j.proeng.2015.08.784](https://doi.org/10.1016/j.proeng.2015.08.784).
- [18] “FLIR LEPTON® Engineering Datasheet”. In: (2019).
- [19] Alfred Gatt et al. “A comparison of thermographic characteristics of the hands and wrists of rheumatoid arthritis patients and healthy controls”. In: *Scientific Reports* 9.1 (2019), pp. 1–8.
- [20] Laure Gossec et al. “Relative clinical influence of clinical, laboratory, and radiological investigations in early arthritis on the diagnosis of rheumatoid arthritis. Data from the French Early Arthritis Cohort ESPOIR”. In: *The Journal of rheumatology* 37.12 (2010), pp. 2486–2492. ISSN: 0315-162X.
- [21] W. Grassi and C. Cervini. “Ultrasonography in rheumatology: an evolving technique. Annals of the rheumatic diseases”. In: *Arthritis Rheumatism: Official Journal of the American College of Rheumatology* 57.5 (1998), pp. 268–271.
- [22] “Guidelines for the management of rheumatoid arthritis. American College of Rheumatology Ad Hoc Committee on Clinical Guidelines”. In: *Arthritis and rheumatism* 39 (), pp. 713–22.
- [23] Qiang Guo et al. “Rheumatoid arthritis: pathological mechanisms and modern pharmacologic therapies”. In: *Bone Research* 6.1 (2018). ISSN: 2095-6231. doi: [10.1038/s41413-018-0016-9](https://doi.org/10.1038/s41413-018-0016-9).

- [24] Kirk J. Havens and Edward J. Sharp. “Chapter 3 - Remote Sensing”. In: *Thermal Imaging Techniques to Survey and Monitor Animals in the Wild*. Ed. by Kirk J. Havens and Edward J. Sharp. Boston: Academic Press, 2016, pp. 35–62. ISBN: 978-0-12-803384-5. DOI: <https://doi.org/10.1016/B978-0-12-803384-5.00003-8>.
- [25] Yasuhiro Hosaki et al. “Non-invasive study for peripheral circulation in patients with diabetes mellitus”. In: 72 (2002), pp. 31–37.
- [26] Britney Jones et al. “Hot joints: myth or reality? A thermographic joint assessment of inflammatory arthritis patients”. In: *Clinical Rheumatology* 37.9 (2018), pp. 2567–2571.
- [27] H König, Juergen Sieper, and Karl-Juergen Wolf. “Rheumatoid arthritis: evaluation of hypervascular and fibrous pannus with dynamic MR imaging enhanced with Gd-DTPA”. In: *Radiology* 176.2 (1990), pp. 473–477. ISSN: 0033-8419.
- [28] Nermin Köşüş et al. “Comparison of standard mammography with digital mammography and digital infrared thermal imaging for breast cancer screening”. In: *Journal of the Turkish German Gynecological Association* 11.3 (2010), p. 152.
- [29] Ray Lawson. “Implications of surface temperatures in the diagnosis of breast cancer”. In: *Canadian Medical Association Journal* 75.4 (1956), p. 309.
- [30] Daniel et al. Lighter. “Detecting inflammation in rheumatoid arthritis using Fourier transform analysis of dorsal optical transmission images from a pilot study.” In: *Journal of biomedical optics* 24.6 (2019), pp. 1–12. DOI: [10.1117/1.JBO.24.6.066008](https://doi.org/10.1117/1.JBO.24.6.066008).
- [31] Gitanjali Mate et al. “Automatic Prediction of Rheumatoid Arthritis Using CNN”. In: Apr. 2022, p. 1.
- [32] Fiona M McQueen et al. “Magnetic resonance imaging of the wrist in early rheumatoid arthritis reveals progression of erosions despite clinical improvement”. In: *Annals of the Rheumatic Diseases* 58.3 (1999), pp. 156–163. ISSN: 0003-4967.

- [33] José Meseguer, Isabel Pérez-Grande, and Angel Sanz-Andrés. *5 - Thermal radiation heat transfer*. Ed. by José Meseguer, Isabel Pérez-Grande, and Angel Sanz-Andrés. Woodhead Publishing, 2012, pp. 73–86. ISBN: 978-1-84569-996-3. doi: <https://doi.org/10.1533/9780857096081.73>.
- [34] J. Morović-Vergles. “[Pathophysiology of rheumatoid arthritis]”. In: *Reumatizam* 50.2 (2003), pp. 15–7. ISSN: 0374-1338 (Print) 0374-1338.
- [35] et al. Newman J.S. “Power Doppler sonography of synovitis: assessment of therapeutic response—preliminary observations.” In: *Radiology* 198.2 (1996), pp. 582–584.
- [36] Mikkel Østergaard. “Magnetic Resonance Imaging in Rheumatoid Arthritis. Quantitative methods for assessment of the inflammatory process in peripheral joints: Summary of Thesis”. In: *Scandinavian Journal of Rheumatology* 28.4 (1999), pp. 265–265. ISSN: 0300-9742.
- [37] Mikkel Østergaard, Bo Ejbjerg, and Marcin Szkudlarek. “Imaging in early rheumatoid arthritis: roles of magnetic resonance imaging, ultrasonography, conventional radiography and computed tomography”. In: *Best Practice Research Clinical Rheumatology* 19.1 (2005), pp. 91–116. ISSN: 1521-6942.
- [38] Mikkel Østergaard, Susanne Juhl Pedersen, and Uffe Møller Døhn. “Imaging in rheumatoid arthritis – status and recent advances for magnetic resonance imaging, ultrasonography, computed tomography and conventional radiography”. In: *Best Practice Research Clinical Rheumatology* 22.6 (2008), pp. 1019–1044. ISSN: 1521-6942. doi: <https://doi.org/10.1016/j.berh.2008.09.014>.
- [39] Mikkel Østergaard et al. “Magnetic resonance imaging-determined synovial membrane and joint effusion volumes in rheumatoid arthritis and osteoarthritis. Comparison with the macroscopic and microscopic appearance of the synovium”. In: *Arthritis Rheumatism* 40.10 (1997), pp. 1856–1867. ISSN: 0004-3591.

- [40] Mikkel Østergaard et al. “Quantification of synovitis by MRI: correlation between dynamic and static gadolinium-enhanced magnetic resonance imaging and microscopic and macroscopic signs of synovial inflammation”. In: *Magnetic resonance imaging* 16.7 (1998), pp. 743–754. ISSN: 0730-725X.
- [41] Pravin Patil and Bhaskar Dasgupta. “Role of diagnostic ultrasound in the assessment of musculoskeletal diseases.” In: *Therapeutic advances in musculoskeletal disease* 4.5 (2012), pp. 341–55. doi: [10.1177/1759720X12442112](https://doi.org/10.1177/1759720X12442112).
- [42] Jolanta Pauk, Mikhail Ihnatouski, and Agnieszka Wasilewska. “Detection of inflammation from finger temperature profile in rheumatoid arthritis”. In: *Medical & Biological Engineering & Computing* 57.12 (2019), pp. 2629–2639.
- [43] PJRC. “Teensy Development board”. In: (2022).
- [44] J. A. Rindfleisch and D. Muller. “Diagnosis and management of rheumatoid arthritis”. In: *Am Fam Physician* 72.6 (2005), pp. 1037–47. ISSN: 0002-838X (Print) 0002-838x.
- [45] Muller D Rindfleisch JA. “Diagnosis and management of rheumatoid arthritis”. In: *American Family Physician* (2005). doi: [https://doi.org/72\(6\):1037-47](https://doi.org/72(6):1037-47).
- [46] Francis Ring. “Thermal imaging today and its relevance to diabetes”. In: *Journal of diabetes science and technology* 4.4 (2010), pp. 857–862.
- [47] P. N. Scutellari and C. Orzincolo. “Rheumatoid arthritis: sequences”. In: *Eur J Radiol* 27 Suppl 1 (1998), S31–8. ISSN: 0720-048X (Print) 0720-048x. doi: [10.1016/s0720-048x\(98\)00040-0](https://doi.org/10.1016/s0720-048x(98)00040-0).
- [48] U Snehalatha et al. “Automated hand thermal image segmentation and feature extraction in the evaluation of rheumatoid arthritis”. In: *Proceedings of the Institution of Mechanical Engineers, Part H: Journal of Engineering in Medicine* 229.4 (2015), pp. 319–331.

- [49] Iwona Sudoł-Szopińska. “Rheumatoid arthritis: what do MRI and ultrasound show”. In: *Journal of ultrasonography* 17.68 (2017), pp. 5–16. doi: <https://doi.org/10.15557/JoU.2017.0001>.
- [50] et al. Szkudlarek M. “Power Doppler ultrasonography for assessment of synovitis in the metacarpophalangeal joints of patients with rheumatoid arthritis: a comparison with dynamic magnetic resonance imaging.” In: *Arthritis Rheumatism: Official Journal of the American College of Rheumatology* 44.9 (2001), pp. 2018–2023.
- [51] et al. Szkudlarek M. “Ultrasonography of the metatarsophalangeal joints in rheumatoid Arthritis: comparison with magnetic resonance imaging, conventional radiography, and clinical examination”. In: *Arthritis Rheumatism: Official Journal of the American College of Rheumatology* 50.7 (2004), pp. 2103–2112.
- [52] YK Tan et al. “Thermography in rheumatoid arthritis: a comparison with ultrasonography and clinical joint assessment”. In: *Clinical Radiology* 75.12 (2020), 963–e17.
- [53] York Kiat Tan et al. “A novel use of combined thermal and ultrasound imaging in detecting joint inflammation in rheumatoid arthritis”. In: *European Journal of Radiology* 134 (2021), p. 109421.
- [54] AI-Thinker. “ESP-12S User Manual”. In: (2016).
- [55] Snehalatha Umapathy, Sowmiya Vasu, and Nilkantha Gupta. “Computer aided diagnosis based hand thermal image analysis: a potential tool for the evaluation of rheumatoid arthritis”. In: *Journal of Medical and Biological Engineering* 38.4 (2018), pp. 666–677.
- [56] Rubén Usamentiaga et al. “Infrared thermography for temperature measurement and non-destructive testing”. In: *Sensors* 14.7 (2014), pp. 12305–12348.
- [57] uweelectronic. “Peltier Modules”. In: () .

- [58] Bertrand Vandeportaele. “A Finite State Machine modeling language and the associated tools allowing fast prototyping for FPGA devices”. In: *2017 IEEE International Workshop of Electronics, Control, Measurement, Signals and their Application to Mechatronics (ECMSM)*. 2017, pp. 1–6. doi: [10.1109/ECMSM.2017.7945900](https://doi.org/10.1109/ECMSM.2017.7945900).
- [59] et al. Wakefield R.J. “The value of sonography in the detection of bone erosions in patients with rheumatoid Arthritis: a comparison with conventional radiography”. In: *College of Rheumatology* 43.12 (200), pp. 2762–2770.
- [60] Quanzeng Wang et al. “Infrared thermography for measuring elevated body temperature: Clinical accuracy, calibration, and evaluation”. In: *Sensors* 22.1 (2021), p. 215.
- [61] Y.Bai. *Practical Microcontroller Engineering with ARM Technology*. 1. Wiley-IEEE Press eBook Chapters, 2016, pp. 19–20.
- [62] S Zheng et al. “MRI bone oedema predicts eight year tendon function at the wrist but not the requirement for orthopaedic surgery in rheumatoid arthritis”. In: *Annals of the rheumatic diseases* 65.5 (2006), pp. 607–611. ISSN: 0003-4967.